REPORT DOCUMENTATION PAGE

AFRL-SR-BL-TR-02-

0718

ng the
ducing
202-
urrently

1. REPORT DATE (DD-MM-YYYY)	2. REPORT TYPE	3. DATES COVERED (From - To)
February 2002	Final	Jan 1998 - Sept 2001

4. TITLE AND SUBTITLE
Closed-Loop Control of Acoustic Tones in Aircraft Cavities

5a. CONTRACT NUMBER
F49620-98-1-0276

5b. GRANT NUMBER

5c. PROGRAM ELEMENT NUMBER

6. AUTHOR(S)
David R. Williams

5d. PROJECT NUMBER

5e. TASK NUMBER

5f. WORK UNIT NUMBER

7. PERFORMING ORGANIZATION NAME(S) AND ADDRESS(ES)

Fluid Dynamics Research Center
Illinois Institute Technology
Chicago IL 60616

8. PERFORMING ORGANIZATION REPORT NUMBER

9. SPONSORING / MONITORING AGENCY NAME(S) AND ADDRESS(ES)
USAF, AFRL
AR Office of Scientific Research
801 N. Randolph St
Arlington VA 22203-1977

10. SPONSOR/MONITOR'S ACRONYM(S)

11. SPONSOR/MONITOR'S REPORT NUMBER(S)

12. DISTRIBUTION / AVAILABILITY STATEMENT

DISTRIBUTION STATEMENT A
Approved for Public Release
Distribution Unlimited

13. SUPPLEMENTARY NOTES

14. ABSTRACT

An experimental investigation of acoustic mode noise suppression was conducted with a cavity model at the U.S. Air Force Academy Subsonic Wind Tunnel. Analog and digital control systems were used to suppress Rossiter tones over the Mach number range 0.25 to 0.5. The effectiveness of different closed-loop control strategies was investigated, including PD type, adaptive and a flow physics based algorithm. Experiments showed the Rossiter modes to have either a strong single-mode character or weak multimode character depending upon Mach number.

20020402 083

15. SUBJECT TERMS
active flow control, acoustic tone suppression, weapons bay cavity

16. SECURITY CLASSIFICATION OF:			17. LIMITATION OF ABSTRACT	18. NUMBER OF PAGES	19a. NAME OF RESPONSIBLE PERSON
a. REPORT	b. ABSTRACT	c. THIS PAGE			David R. Williams
					19b. TELEPHONE NUMBER (include area code) (312)-567-3192

Closed-Loop Control of Acoustic Tones in Aircraft Cavities

FINAL REPORT

(January 1998 – September 2001)

Prepared by

David R. Williams

Fluid Dynamics Research Center
Illinois Institute of Technology
Chicago, Illinois 60616

For

Air Force Office of Scientific Research

Contract F49620-98-1-0276

RESEARCH SUMMARY

Title: Closed-Loop Control of Acoustic Tones in Aircraft Cavities

Contractor: Illinois Institute of Technology
Contract F49620-98-1-0276

Principal Investigator: David R. Williams

Report Period: January 1998 – September 2001

Objective: To investigate flow physics associated with large amplitude acoustic tones in aircraft cavities, and study closed-loop control architectures to reduce those tones

Technical Perspective: Weapons bays in modern aircraft are known to develop acoustic resonances with sound pressure levels greater than 160dB at subsonic flight Mach numbers. Closed-loop active flow control techniques may outperform traditional passive methods of suppressing the tones. Better understanding of the flow physics responsible for the resonance process will provide improvements in the control system.

Technical Approach: Efforts at IIT and Caltech developed both analog and digital closed-loop control systems to suppress acoustic tones. The performance of the different systems was studied in the U.S. Air Force Academy Subsonic Wind Tunnel facility. The fundamental flow physics of the acoustic resonance process were studied.

Results: The experiments identified two types of resonances that were dependent on Mach number, namely single mode and multimode types. The effectiveness of control algorithms ranging from simple PD-type to adaptive and flow-physics based algorithms were examined. The digital controllers were comparable to a simpler analog controller in the degree of noise suppression achieved (typically 18 dB) with single mode resonance. However, the digital controllers were not able to suppress multiple modes simultaneously. An empirical model representing cavity flow physics was developed. The physics based model was successful in suppressing specific modes, and provided a logical framework to improve control models. The experiments showed single-mode resonance at M=0.34 to be self-excited and in a nonlinearly saturated limit-cycle state. In contrast, nonlinear effects do not saturate the multimode resonance states occurring at other Mach numbers. Input disturbance levels from external sources determine the amplitudes of the multimode resonances.

Table of Contents

Abstract 4
Nomenclature 4
1. Introduction 5
1.a Background 5
1.b Physics of the Resonance Mechanism 6
1.c Overview of the Digital Control Approach 7
2. Experimental Arrangement 8
3. Results 10
3.a Boundary Layer 10
3.b Acoustic Modes 10
3.c Shear Layer 11
3.d Actuator input to shear layer 12
3.e Analog Feedback Control Experiments 12
3.f Adaptive Digital Control Experiments 13
3.g Control based on flow physics model – (Shear layer and Open Loop Forcing) 14
4. Discussion of Results 16
4.a Comparison of analog vs. digital control systems 16
4.b Self-excited modes vs. turbulence driven modes 16
5. Conclusions 17
6. Acknowledgements 18
7. References 18
8. Appendix 37
9. Figure List 43

Abstract

An experimental investigation of acoustic mode noise suppression was conducted with a cavity model at the U.S. Air Force Academy Subsonic Wind Tunnel facility. Flow Mach numbers ranging from 0.25 to 0.55 were studied. The experiments identified two types of resonances, namely single mode and multimode types. In addition to experiments investigating flow physics, closed-loop feedback control experiments were done using analog and digital control systems. The effectiveness of control algorithms ranging from the simple PD-type to adaptive and flow-physics based algorithms were examined. The adaptive controller was comparable to a simpler analog controller in the degree of noise suppression achieved with single modes. Typical noise suppression levels varied from 15 dB to 18 dB. In contrast to the analog controller, the digital controllers were not able to suppress multiple modes simultaneously. To explore the reasons for the limitations in controller performance, a new empirical model representing cavity flow physics was developed in collaboration with Professors Tim Colonius (Caltech) and Clancy Rowley (Princeton). The physics based model was successful in suppressing specific modes, and provided a logical framework to improve control models. The experiments showed single-mode resonance at M=0.34 to be self-excited and in a nonlinearly saturated limit-cycle state. In contrast, nonlinear effects do not saturate the multimode resonance states occurring at other Mach numbers. Input disturbance levels from external sources determine the amplitudes of the multimode resonances.

Nomenclature

C_p = Pressure coefficient $(p-p_1)/q$
D = Cavity depth
f = Frequency
L = Cavity length
M = Freestream Mach number
p_1 = Wind tunnel static pressure
q = Dynamic pressure $\frac{1}{2} \rho U_o^2$
St = Strouhal number, fL/U_o
U_o = Freestream speed
W = Cavity width
ρ = air density
γ = Coherence function

1. Introduction

1.a Background

Open cavities on aircraft are known to produce large amplitude tones, which may adversely affect performance of the flight vehicle. Investigations into the nature of the resonant tones within aircraft cavities have been conducted since the 1950's[1,2]. At flight Mach numbers as low as M=0.5 pressure fluctuations in the weapons bay and wheel well cavities can exceed 160dB, which can cause early structural failures and produce additional drag on the aircraft. Ordnance in the weapons bay may experience adverse structural loads due to the unsteady forces, and changing flow patterns in the cavity may lead to unpredictable store separation trajectories. Overall aircraft drag is substantially increased during resonant conditions, because the cavity drag can increase as much as 250% above non-resonant conitions[3]. The "cavity problem" is a challenging case for flow control, because of the changing flow conditions during flight and the coupling of the cavity flow with store separation behavior[4].

Techniques to reduce the occurrence of resonant tones fall into two general categories, passive and active. Passive techniques include rods, spoilers or flaps at the leading edge of the cavity, ramps and contouring the downstream wall. These techniques usually have a limited range of effectiveness and may increase noise levels at off-design conditions. Pinney and Leugers[4] observed that the performance of passive sound suppression devices can be sensitive to Mach number, thereby limiting the range of their effectiveness, and enhancing certain acoustic tones at off-design conditions. For these reasons, active control schemes that are capable of adjusting to changing cavity flow conditions are being explored[5,6]. The consortium known as Active Robust ConTrol of Internal Cavities[7] (ARCTIC) was formed in 1998 to study the feasibility of developing an active control system capable of suppressing tones in a weapons bay cavity, then to flight test the system on an F-111G.

Active flow control techniques have been explored recently as possible replacements for the passive approach[5,8-11]. The active techniques can be either open-loop or closed-loop. Active control introduces additional energy to the flow through an actuator, and can be turned on and off as needed. They can be tailored to a particular flight condition giving a wider range of effectiveness. If the energy addition to the flow from the actuator is not directly coupled to some flow parameter, then it is the "open-loop" type. Many different types active control techniques have been explored as potential cavity acoustic controllers. A partial list of control actuators that have been tested include steady and unsteady jets[8], piezoelectric flappers[9,12], fluidic oscillators[10], unsteady bleed forcing[11,13]and high-frequency excitation (Hifex.) The majority of these have been open-loop experiments, primarily designed to evaluate the effectiveness of the actuator in modifying the flow or reducing noise. Closed-loop control for the cavity problem was demonstrated by Cattafesta, et al.[9] at low Mach numbers (M = 0.2) and by Shaw[8] at higher Mach numbers.

Closed-loop control uses a flow state sensor (typically pressure or velocity) modified by a control algorithm to produce a feedback signal that drives the actuator. The closed-loop control approach is the most complicated of noise suppression techniques, but offers the advantages of low power requirements, and adaptability to changing flow conditions. Cattafesta, et al.[9] demonstrated the substantial power efficiency that could be achieved with a feedback controller.

Because the acoustic modes to be suppressed are Mach number dependent[14], the cavity flow is a candidate for adaptive control. Changes in flight conditions require the controller to adapt to new mode characteristics in order for the noise suppression to be effective. Even at a fixed Mach number, the acoustic energy will shift from one mode to another. The group at High Technology[9] and Kegerise[15] observed the energy exchange among various Rossiter modes in uncontrolled cavities. A controller that is capable of tracking and suppressing the various modes could be very efficient, requiring low power levels to suppress the tones.

1.b Physics of the Resonance Mechanism

The cavity supports at least three distinct instabilities; namely, the normal acoustic modes between the cavity walls, the wake mode, and the Rossiter modes. Rossiter[14] recognized that the unsteady flow in the shear layer over the cavity provided the forcing necessary for the resonance mechanism, rather than the turbulence in the boundary layer. The resonance occurred when the vortex shedding from the upstream edge produced periodic acoustic waves that matched the natural frequency of the cavity. By equating the total time for wave propagation to the period of oscillation, Rossiter obtained the empirical equation

$$St = \frac{fL}{U_0} = \frac{m - \gamma}{\frac{1}{\kappa} + \frac{M}{\sqrt{1 + \frac{\gamma - 1}{2} M^2}}} \qquad \text{(eqn. 1)}$$

for predicting the discrete frequencies that appear under compressible flow conditions. The model has been shown to be reasonably accurate at a large number of test facilities, provided the two parameters γ and κ are adjusted properly. The constant κ is the shear layer vortex convection speed (normalized by U_0) and γ is associated with the velocity-pressure phase delay occurring during the scattering process. Dix & Bauer[16] showed the dependence of γ on the cavity aspect ratio L/D and initial shear layer thickness.

Bilanan & Covert[17] and Tam & Block[18] made improvements to the conceptual model, which accounted for the effects of feedback path length, shear layer instability, finite shear layer thickness and cavity depth. However, none of these models could predict amplitudes of modes or even the relative distribution of energy among the various modes. In an attempt to estimate the distribution of energy among the various modes, the linear stability of the shear layer was considered in the investigations of Sarohia[19], and Hankey & Shang[20]. The latter study used the amplification rates from linear stability analysis to predict the relative intensities of the acoustic tones, and they found reasonable agreement with experiment at one Mach number. A mechanism for nonlinear saturation of disturbances was included in a numerical simulation package (CAMS) developed by Cain, et al.[21] The CAMS model does make predictions of both mode amplitude and frequency.

Designing an effective closed-loop controller requires some understanding of the flow field physics responsible for the resonance. The success of the Rossiter model in predicting the frequencies gives confidence that the basic physics of the resonance mechanism are correct. To design an active feedback control system capable of suppressing the tones is feasible, if the actuator can modify or disrupt the resonant feedback loop.

The work at IIT/FDRC concentrated on designing a series of controllers beginning with a simple analog system in the first year followed by a digital system, a flow-physics algorithm, and digital adaptive system in the last two years. To concentrate the effort on the development of closed-loop control systems, the actuator was kept essentially constant throughout most of the work. Initial work was done in the first year to design a wide-bandwidth actuator capable of suppressing the first four Rossiter tones. The actuator design was kept fixed for the remainder of the tests except for small changes in nozzle geometry. The actuator performance and the response of the cavity flow to the actuator forcing were documented using pressure sensors and hot-wire anemometers. The second year effort investigated digital and adaptive digital control. Lessons learned from the first two years motivated the need for better understanding of the physics. In the final year the IIT group combined efforts with Colonius and Rowley[22] at Caltech to bring their experience with control systems and numerical simulations to the problem. An approach based on flow field physics was used. During this phase of the research Rowley discovered that certain Rossiter modes appear to be self-induced (absolute or globally unstable), while others will damp without an input of energy. The flow physics model provided new guidance and insight into the resonance mechanism, fundamental limitations on achievable control, and provided a framework for developing new control approaches.

1.c Overview of the Digital Control Approach

Before describing the details of the experiment, it is worth describing some advantages of digital control. Recent developments in digital signal processor (DSP) technology have made it feasible to transition sophisticated control algorithms from the laboratory to practical flow control applications. The small physical size of DSP's and their low cost are attractive features for aerospace applications. Onboard memory of the order 100 kilowords and processing speeds at 75 mips are more than adequate to support algorithms fast enough to suppress tones in the kiloHertz range. Throughout the course of this work two commercial DSP systems and a variety of different control algorithms for suppressing resonant tones in a cavity were used successfully, demonstrating the practicality of DSP technology for flow control.

The adaptive control system was a commercial active noise control package from Arbor Scientific[23] that was chosen in this experiment for its flexibility and ease of implementation. The control algorithm consisted of three basic components, 1) a digital control filter, 2) the cancellation path model and 3) the adaptive algorithm. The controller required two input signals in the adaptive feed-forward architecture; namely, the reference signal and the error signal. A block diagram of the feed forward control approach is shown in Fig. 1 for the cavity. The reference signal is processed by the control filter to generate the feedback signal. A recursive-type (infinite impulse response) filter was chosen for this application, because it more accurately simulates the feedback in the physical system. Some tests were done with an FIR-type filter, but the filter had to be much larger and required longer computation times to achieve the same degree of noise suppression that was possible with the recursive filter.

In a conventional application the feed forward control system uses a reference signal to measure the disturbance upstream of the actuator. The control system computes the appropriate actuator response required to cancel the incoming disturbance. An error signal is obtained from

a sensor located downstream of the actuator, which measures the residual disturbance after the actuator has acted. The error signal is a combination of the disturbance, the actuator produced disturbance and intermediate noise. Because the cavity resonance mechanism involves upstream travelling acoustic waves that form a feedback loop within the flow, the cavity does not have clearly defined upstream and downstream locations for the feed forward algorithm. Consequently, the reference signal will always detect some percentage of the actuator signal, which can cause the control system to become unstable at high system gains.

The purpose of the adaptive algorithm is to adjust the control filter coefficients in a way to minimize the error signal amplitude. The Arbor Scientific software uses the filtered-x least-mean-square gradient descent algorithm to search for optimized filter coefficients. The adaptive algorithm requires information from the cancellation path model to calculate the local gradient of the error surface in filter coefficient space. The cancellation path model tries to predict the response of the cavity flow to the actuator input. This information is used by the adaptive algorithm to correct the direction for modifications to the control filter coefficients. As the filter coefficients are updated, the magnitude of the error signal should progressively decrease until it is minimized. When the flow conditions are steady, then the optimized filter coefficients become constants. If the flow state changes due to a change in flight conditions or a shift of acoustic energy to a different resonant mode, then the adaptive algorithm will readjust the control filter coefficients.

The cancellation path model is the third basic component of the adaptive controller, and simulates the system from the feedback signal to the actuator, through the shear layer to the error signal input. If a plant model for the system existed, then it would be the major component of the cancellation path model. Unfortunately, at the present time there is no suitable plant model, although efforts are underway by Rowley, et al.[22] to develop a low-dimensional model based on flow field physics for control applications. Without a cancellation path model based on flow physics, it becomes necessary to use system identification techniques as an approximation. Pillarisetti, et al.[24] and Cattafesta, et al.[25] have explored these methods. The Arbor Scientific software uses a finite impulse response filter for the cancellation path model. A gradient descent algorithm is used to optimize the filter coefficients by minimizing the error between the model and the actual cavity response. The result is a cancellation path model that can be used by the adaptive algorithm.

2. Experimental Arrangement

The cavity control experiments were conducted in the U.S. Air Force Academy Subsonic Wind Tunnel. The wind tunnel has cross-section dimensions of 0.91m x 0.91m (3 ft. x 3 ft.) The empty Subsonic Wind Tunnel is capable of speeds up to M = 0.6, although the drag of the cavity limited the achievable Mach number to 0.55. The cavity model was mounted in the floor of the wind tunnel test section. The cavity width was W = 0.38m (15 in.) and its length was L = 0.51m (20 in.) Although the depth of the cavity could be varied, it was fixed at D = 0.096m (4 in.) for the majority of the experiments giving an aspect ratio L/D = 5. A photograph of the cavity mounted in the wind tunnel is shown in Fig. 2.

The cavity was instrumented with eight Kulite sensors (model XCS-093) positioned from the front wall to the rear wall along the centerline of the cavity as shown in Fig. 3. The signals were bandpass filtered through fourth-order Butterworth filters with a passband of 0.4 Hz to 2.2 kHz. All analog signals were sampled at 6,000 samples/(second-channel.)

Controller hardware and software was purchased from Arbor Scientific. The DSP platform of the system is an Analog Devices ADSP 2181 evaluation board. The system was run at 1375 samples/second with a 690 Hz low pass filter, which resulted in generally stable operation. The reference and error signals to the controller were taken from two Kulite sensors in the cavity.

A simple analog control system was used as a benchmark to judge the adaptive control performance. The analog control system used a single Kulite pressure sensor as its input. The signal was narrow bandpass filtered about individual Rossiter modes with three Ithaco 4212 filters to create three feedback signals. Each feedback signal was phase-shifted through a manually controlled circuit constructed at IIT. The three signals were recombined with an adding circuit, then sent to a 900 Watt Fender power amplifier to drive the actuator.

The actuator for both analog and digital systems consists of a pair of 500 Watt, 8-inch Pyramid loudspeakers. The loudspeakers are enclosed in an aluminum housing to equalize the pressure surrounding the speaker cone with the wind tunnel test section pressure. This was essential to obtain good performance from the actuator. The actual power required by the actuators varied from 1 to 53 Watts depending on specific flow conditions. The transfer functions for the velocity and pressure responses of the actuators were measured with a hot-wire anemometer (Disa model 55D) and Bruel & Kjaer microphone. The response functions of the actuator are reproduced in Fig. 4 from Ref.[26]. The cutoff frequency of the actuator occurs at 600 Hz.

3. Results

3.a Boundary Layer

Measurements of the separating boundary layer were made with a small pitot tube at Mach numbers ranging from 0.2 to 0.55. The profile was typical of a turbulent boundary layer. The values of the boundary layer thickness at $0.995U_o$ and the momentum thickness are listed in Table I.

Table I – Boundary Layer and Momentum Thickness at Upstream Cavity Wall

Mach	$\delta_{99.5}$ (cm)	θ (cm)
0.2	3.18	.30
0.25	3.05	.28
0.3	2.79	.29
0.35	2.79	.28
0.4	2.54	.27
0.45	2.54	.27
0.5	2.41	.27
0.55	2.41	.26

3.b Acoustic Modes

The spectral peaks measured by a Kulite transducer mounted in the upstream cavity wall are plotted against the Mach number in Fig. 5. The solid lines are predictions using the Rossiter formula where the parameter κ=0.625 represents the shear layer vortex convection speed normalized by freestream speed. The data show at least four Rossiter modes appearing at different Mach numbers.

The Rossiter plot shown in Fig. 5 does not give the complete picture about which modes are dominant or how the energy is distributed. To study the changes in energy among the different modes, the wind tunnel Mach number was increased in small steps of M= 0.025. Rather rapid changes in the spectral energy content were observed. A small set of spectra are shown in Fig. 6 corresponding to the L/D = 5 cavity. The spectra for a Kulite transducer located in the upstream wall of the cavity were obtained at M = 0.25, 0.275, 0.35 and 0.375 and are shown in Figs. 6a,b,c and d, respectively. At M = 0.25 and M = 0.35 (Figs.6a and 6c) a single strong peak dominates the spectrum, and the cavity is said to be in single-mode resonance. After increasing the Mach number by the small increment of 0.025 to M = 0.275 and M = 0.375, the resonance changes to the multimode type. The amplitudes of the spectral peaks drop significantly when the multimode behavior begins. As shown by Cattafesta, et al. and Williams, et al. the energy switches back and forth among the various Rossiter modes during multimode resonance.

The data in Fig. 7 show the Rossiter modes superposed with two normal cavity modes and one mode corresponding to a transverse test section mode in the wind tunnel. The latter mode is

an order of magnitude weaker than the cavity modes. The Mach numbers at which single mode resonance occurs are located at the intersections of the first longitudinal cavity mode with the second, third and fourth Rossiter modes. Rockwell and Naudascher[27] were the first to recognize the possible coupling between these modes. However, as Kegerise points out, the coupling does not predict all the dominant modes. The Mach numbers for multimode resonances fall between the single-mode resonances. In the range $0.375 < M < 0.45$, a large number of spectral peaks were observed. Energy is continuously being exchanged from one Rossiter mode to another, and no single mode locks-in to dominate the spectrum.

3.c Shear Layer

The shear layer development over the cavity is one of the primary elements of the resonance process. It determines the convective speed of the vortices (vortical waves), the growth rates and saturation amplitudes of the vortical waves. The shear layer acts like a filter/amplifier to the broadband turbulence from the boundary layer and feedback pressure signal that defines the Rossiter mechanism. Tam & Block[18] discussed the importance of finite shear layer effects and incorporated it into their model of the cavity physics. They point out that shear layer growth rate is related to disturbance amplitude, and the two are coupled. Lacking detailed measurements they were forced to use an average value of the momentum thickness. Hankey & Shang[20] used disturbance growth rates from stability theory to predict the relative amplitudes of the Rossiter modes. Detailed measurements of a cavity shear layer were made by Kegerise[15] using hot-wire anemometers and a novel quantitative schlieren technique (optical deflectometry.) His experiments showed that the relative magnitudes of the Rossiter modes did not correspond to the predictions of linear stability theory, but were determined by the shear layer mode amplitudes at the downstream end of the cavity.

Measurements of the shear layer growth over cavities are somewhat limited. Sarohia[19] studied the flow over an axisymmetric cavity and found momentum thickness growth rates to be as high as $d\theta/dx = 0.022$. Oster & Wygnanski[28] studied the development of free shear layers (without a cavity) under forced and unforced conditions. Their results showed the growth rate of the unforced free shear layer depends upon the velocity ratio $r = U_1/U_2$. As the velocity ratio varied from $r = 0.3$ to 0.6, $d\theta/dx$ decreased from 0.019 to 0.0085. In the case of a shear layer forced with an oscillating flap Oster & Wygnanski found three separate regions of momentum thickness growth. Region I has a linear growth rate that exceeds the unforced case. In region II the growth rate slowed or even became negative at high forcing amplitudes. From flow visualization they determined that the normal vortex amalgamations are inhibited in region II. The growth rate in region III became linear again at a rate close to that in region I as vortex amalgamations reoccur.

Hot wire measurements of the shear layer velocity profiles are shown in Fig.8a for $x/L = 0.1$ to 0.6. The y-coordinate is normalized by the vorticity thickness $\delta_\omega=(U_2 - U_1)/dU/dy|_{max}$. The velocity deficit $U(y)-U_1$ was normalized by (U_2-U_1), where U_1 was determined to be approximately $0.12U_2$ by curvefits to the data. It is recognized that measurements of the low velocity region in the cavity are problematic due to the reversed flow. The corresponding r.m.s. velocity profiles are shown in Fig. 8b.

Growth of the shear layer is shown in Fig. 9 with and without mode suppression with the control system. The analog control system was used to suppress the resonant mode by 7dB. Essentially negligible difference is found between the forced and unforced cases. The data show a region of near zero growth between x/L = 0.1 to 0.2, which is similar to region II found by Oster & Wygnanski.

3.d Actuator input to shear layer

Open loop forcing experiments were conducted at M=0.34 to determine the response of the shear layer and cavity system to changing input amplitudes. The shear layer response was measured with a hot-film probe at x/L = 0.031, y=0. The forcing frequency was fixed at 380 Hz. The linear response of the shear layer velocity responds to the voltage input to the actuator can be seen in Fig. 10a. The pressure response in the cavity relative to the velocity fluctuation level in the shear layer is shown in Fig. 10b, and can be seen to have a nonlinear behavior.

3.e Analog Feedback Control Experiments

The signal from a Kulite sensor located in the upstream wall was used as an error signal in the feedback control system. A block diagram of the analog control system is presented in Fig. 11. The signal was narrow bandpass filtered to allow only a small portion of the acoustic spectrum to be sent to the actuator. Fig. 11 presents a block diagram of the analog control system. The first objective was to demonstrate the ability to influence the shear layer development and the acoustic field resulting from the impingement of the unsteady shear layer on the downstream cavity wall. The effect of feedback signal phase changes on the acoustic field were to be documented for use in designing the feed-forward control system

The first example of a closed-loop control case is shown in Fig. 12, where only one frequency dominates the spectrum at 340Hz. The data correspond to M = 0.34, L/D = 5 with the phase shift circuit adjusted to provide maximum attenuation with the feedback signal. Under these particular flow conditions the majority of energy in the uncontrolled cavity resonance occurred at the second Rossiter mode with amplitude of 148 dB. The 18 dB reduction is slightly higher than obtained with the digital approach, and will be discussed later. A harmonic near 700 Hz was also reduced by the control. In general, the closed-loop control was more effective in the shallower L/D =5 cavity than the deeper cavities with L/D = 4 and L/D = 2.

The phase shift circuit enabled the operator to "dial in" phase lags of the feedback signal from 0° to 360° relative to the Kulite state sensor signal. Therefore, the feedback signal could be manually tuned to reinforce a particular resonant mode or to suppress it.

An example of mode *enhancement* is shown in Fig.13 for M = 0.5 conditions. The filter passband was set to pass frequencies from 250 Hz to 315 Hz, which allowed the second Rossiter mode (labeled 'B') to be increased by 6dB. The third Rossiter mode (labeled 'C') is suppressed when B is enhanced even though it is outside of the frequency range of the actuator. This suggests that a physical connection exists between the B and C modes. It will be shown later that the enhanced energy in mode B indicates that the mode is present for a longer period of time during the integration over the data record.

The effect of adjusting the feedback signal phase to suppress mode 'B' is shown in Fig. 14. The second mode is suppressed 12 dB, while the neighboring mode 'C' is slightly enhanced. The fourth mode 'D' is suppressed by 5dB. Again it should be noted that modes C and D are outside the frequency band of the actuator, and are responding to changes in the cavity flow conditions due to the suppression of mode B.

By shifting the passband to the 400 Hz to 500 Hz range, the third Rossiter mode 'C' can be suppressed. The result as shown in Fig. 15 is similar to the effect of suppressing mode 'B'; namely, the second Rossiter mode is enhanced. A small decrease in the first Rossiter mode 'A' is detectable.

Multiple passbands were setup in an attempt to suppress more than one mode simultaneously. Two Ithaco filters were used in parallel to create two feedback signals in the ranges 200 – 315 Hz and 400-500 Hz to suppress modes 'B' and 'C', respectively. Approximately 7 dB of reduction in each mode was obtained as shown in Fig. 16. The fourth mode 'D' was also reduced by a smaller amount. Separate phase shift circuits were required for each feedback signal, because the amount of phase shifting (or tuning) is different for each mode.

3.f Adaptive Digital Control Experiments

The analog control experiments demonstrated the ability of the cavity to shift energy among various modes. Suppression of one mode would lead to enhancement of another. An adaptive control approach was investigated as possible control architecture for suppressing multiple modes. The adaptive algorithm was discussed earlier and a block diagram of the controller was shown in Fig. 1. The first application of the controller was at M=0.34 for the single mode resonance case. The cancellation path model and the complex coefficients used by the control filter are shown in Fig. 17. By taking the Fourier transform of the cancellation path model we find a single peak at 340Hz, which is consistent with the single mode resonance. The control filter model has two dominant frequencies corresponding to the 340Hz mode and its harmonic. The adaptive control system was capable of suppressing the resonant mode at f = 340 Hz by 15 dB as shown in Fig. 18.

The coherence function measures the degree of correlation between two signals as a function of frequency. The coherence between the reference signal and the feedback signal was $\gamma = 0.97$ prior to activating the sound suppression is shown in Fig. 19. Once the controller reduces the sound level, the flow field has been modified. The coherence at maximum suppression drops to $\gamma = 0.6$. The coherence can be related to the accuracy of the phase measurement. Clearly there is less correlation between the reference signal and the feedback to the actuator, which may explain the poor performance.

When the flow is increased to M = 0.48, then multiple modes appear in the spectrum as shown in Fig.20. The challenge for the adaptive controller is to suppress more than one mode simultaneously. The controller suppressed the second Rossiter mode at 350 Hz, but the energy shifted to the third mode at 475 Hz. The coherence function showed the third mode to have a

very high value $\gamma = 0.9$. Therefore the actuator must have been feeding energy directly into the third mode while suppressing the second.

3.g Control based on flow physics model – (Shear layer and Open Loop Forcing)

The inability of the digital adaptive controller to outperform the analog controller was somewhat surprising, and forced reconsideration of the effort to implement digital control architectures. In the final year of the contract a new direction was taken to involve algorithms based on flow physics. The idea was to take a step back in terms of sophistication, with the objective of gaining more understanding of the effect of the controller on the flow field itself. It was expected that these investigations would explain the limitations on the level of suppression that could be achieved with a given controller. To execute such an experiment required the combined efforts of the IIT experimental group and the computation simulation/controls group at Caltech. The Caltech group consisting of Clancy Rowley, Tim Colonius, Doug MacMartin and Richard Murray had been exploring POD simulations of the cavity flow. It was not feasible to design a control experiment using POD methods within the time available for experiments to be conducted at the US Air Force Academy, but Rowley was able to design a linear model containing the essential physics of the Rossiter modes. The model was implemented in a dSPACE digital control system for use in the laboratory environment.

Fig. 21 presents a block diagram of Rowley's model reproduced from Ref[22]. The model is based on Rossiter's mechanism consisting of transfer functions for disturbance amplification in the shear layer, vortex-sound scattering, normal acoustic modes, and receptivity (sound to vorticity wave conversion.) A combination of theory and experiments was used to obtain transfer functions for each of the components in the model.

The conventional description of the cavity resonance process is that it will selectively amplify specific modes that grow until an equilibrium limit-cycle state is reached. Since we are not conducting transient experiments, the data are obtained with the shear layer in an equilibrium state. To be able to study the shear layer receptivity, the closed-loop control system is used to suppress the resonant mode. Simultaneously open-loop forcing with the actuator is used to inject a controlled disturbance at a frequency slightly detuned from the resonant mode. The development of the open-loop mode is then followed around the resonance loop in the cavity. For example, at M=0.34 the principal resonant mode occurs at 340Hz. This mode is suppressed by 10dB with the feedback controller, and then the actuator is driven in open loop at 380Hz. The 380Hz mode is detuned from the Rossiter resonance mechanism, hence it is not self-excited and does not saturate. Because the principal resonant modes are not completely suppressed, the detuned disturbances are developing on top of a flow field that is not in its pure base state. Nevertheless, as shown from the shear layer velocity profiles, the differences are not large between the suppressed state and the limit-cycle state.

The response of the shear layer is measured with the two hot-film probes located at y=0, $x/L = 0.031$ and 0.92. The transfer function and phase as a function of the open-loop forcing signal are shown in Fig. 22. The shear layer shows higher gains at 220 Hz and 370 Hz than at the 340Hz principal Rossiter mode.

The scattering transfer function represents the conversion of vorticity waves in the shear layer into pressure fluctuations of the acoustic field. This process occurs at the downstream end of the cavity as vortices impinge on the downstream wall. A comparison of the downstream hot film signal with a nearby Kulite pressure transducer located in the downstream wall is shown in Fig. 23. Unfortunately, the acoustic feedback at the open-loop forcing frequency is also present in the pressure transducer signal, which contaminates the results to some degree and may explain the large gain at 340Hz.

The acoustic feedback transfer function was an addition not included in Rossiter's original model, but was determined to be important in the mode selection process. The upstream propagation of the acoustic waves was divided into the "reflection" and upstream propagation. The reflection is a measure of the wave propagating from the downstream edge of the cavity to the floor of the cavity. In this experiment the distance was 127mm. The gain and phase for this component of the resonant loop are shown in Fig. 24.

Receptivity refers to the response of the shear layer to external disturbances, or to the conversion of acoustic disturbances into vortical waves in the shear layer. The shear layer receives input disturbances from at least three sources, namely the turbulent boundary layer, the feedback acoustic wave and the actuator. The boundary layer has a broad spectrum of vortical disturbances to drive the instability. In the cavity problem there is an additional input from the acoustic field to be considered. This includes the acoustic waves that feedback from the shear layer impinging on the downstream wall of the cavity. The third source in the case of control of cavity flows is from the actuator. The actuator introduces disturbances into the shear layer from the controller feedback path.

To obtain a measure of the receptivity transfer function it is necessary to separate the contribution from the actuator to the hot-film signal at the upstream end of the cavity. First the transfer function was computed with the pressure signal in the upstream wall as input, and the hot-film probe velocity signal at $x/L = 0.031$ as output. Next the output of the actuator was computed using the feedback voltage signal and the actuator transfer function to obtain the term to be subtracted from the first transfer function. The results are shown as the gain and phase corresponding to the open-loop forcing frequencies in Fig. 25.

4. Discussion of Results

4.a Comparison of analog vs. digital control systems

The performance of the adaptive digital control system has been examined by comparing its performance against an analog controller. In the case of the single mode resonance the degree of noise suppression with the digital control is comparable. The system identification process worked well to produce a control path model that simulated the cavity in its resonant state prior to suppression. The adaptive control was not able to adjust to changes in flow state, such as Mach number changes. So long as single mode conditions remained steady, the controller was able to configure the control filter effectively. Suppression levels of 15dB were typical.

The digital adaptive control was not as effective as the multi-band analog control. When multiple modes were present, the adaptive algorithm would configure the control filter to suppress one of the modes, but the others were not suppressed and usually increased in magnitude. The phase between the reference signal and the feedback signal was not correctly adjusted for mode suppression, and the energy from the actuator actually enhanced the neighboring modes. The presence of multiple modes in the spectrum is an indication of mode switching as discussed by Cattafesta, et al. and Williams, et al. This may have contributed to the inability of the adaptive algorithm to configure the control filter for multi-mode suppression. Since the adaptive algorithm takes several seconds to converge, and the mode-switching takes place at least an order of magnitude faster, then the resulting control filter coefficients will be a weighted average between the different mode states.

Once the actuator is activated to begin noise suppression, the phase between the feedback and reference signals changes. As a result the actuator becomes detuned from its optimum phase for suppression, and the noise suppression becomes less effective.

4.b Self-excited modes vs. turbulence driven modes

During post processing of results obtained for the flow physics control algorithm, Rowley[22] observed a fundamental difference between the single mode and multi-mode resonance case. Spectra, Poincare plots and probability densitiy plots of the pressure signal shown in Fig. 26 for M = 0.34 and M = 0.45. The limit-cycle behavior of the mode at M = .34 is clearly seen in the Poincare plot, and a random distribution is seen for M = 0.45. The probability density plot also indicates a bimodal shape characteristic of limit cycle behavior of the resonance at M=0.34, and a Gaussian distribution for M=0.45. The implication for the single mode at M = 0.34 is that the mode is self-excited and has amplified until it is in a nonlinearly saturated state. By increasing the Mach number to 0.45, the multiple mode state obtains. In contrast to self-excited modes, these modes do not reach a limit cycle or nonlinearly saturated state. It is believed that turbulence from the boundary layer and acoustic waves near the Rossiter frequencies are amplified in the shear layer. The normal modes of the cavity are not coincident with the Rossiter frequencies at this Mach number, which may explain why a self-excited state is not reached.

5. Conclusions

An experiment using different types of analog and digital closed-loop controllers to suppress and enhance various acoustic modes in a cavity has been conducted in the subsonic wind tunnel at the U.S. Air Force Academy. A simple analog control system has been used to suppress both individual and multiple acoustic modes over a Mach number range of 0.2 to 0.55. The actuator for the control system is a zero-net-mass addition type that uses loudspeakers in an air-tight enclosure. The baseline data (without control) show good agreement between the frequencies present and the well-known Rossiter formula. Large variations in the distribution of energy among the frequencies were seen depending on the cavity depth and Mach number.

Closed-loop control with narrow bandpass filtering was shown to be effective in modifying individual acoustic modes. Using this as a diagnostic technique, nonlinear interactions between different resonant modes have been demonstrated. In the uncontrolled case there is a competition between modes for the energy, and when one mode is suppressed then the energy goes more consistently into the other modes. From an applications perspective, the closed-loop control has been shown to be capable of suppressing multiple modes simultaneously. This is an essential component in the development of a practical adaptive controller for aircraft applications.

A commercial adaptive noise control package that uses a digital signal processor was configured to suppress acoustic modes in a cavity under compressible flow conditions. The digital control performance was compared to a simple analog controller. The performance of the digital controller was comparable to the analog approach when a single resonant tone was present in the experiment. However, at Mach numbers where multiple acoustic modes appeared, the digital controller did not perform as well as the analog controller. In particular, the digital system would usually suppress only one mode and enhance neighboring modes by an equivalent amount. A closer look at the components in the control algorithm showed that the system identification process correctly identified the modes present in the experiment. However, the flow field readjusted to the actuator input so that at least one mode was amplified. The failure of the controller to correctly adapt to changing flow conditions was traced to the inflexible control path model. Either the control path model must be updated during the time the noise is being suppressed, or a model based on flow field physics will be needed to achieve higher levels of noise suppression.

Hot wire measurements of the shear layer development over a cavity showed similarities with forced free shear layer measurements. For comparison closed-loop control was used to suppress the resonant mode by 7dB, and no significant differences in shear layer development were found.

A novel approach to measuring transfer functions of the various flow components that make up the cavity resonance mechanism was attempted. Using Rossiter's[11] model for resonance as a guide, the cavity flow was decomposed into five components representing 1) vortical waves in a shear layer, 2) scattering of vortices from the downstream edge to produce pressure waves, 3) reflection of the acoustic wave to the floor of the cavity, 4) upstream propagation of the acoustic wave through the cavity to the upstream wall, and 5) receptivity of

the shear layer to the pressure waves. Closed-loop control was used to suppress the cavity resonance by 10dB. Simultaneously, open-loop forcing was used to introduce a new frequency into the shear layer. The response of the cavity components was documented in the form of transfer functions with phase plots as functions of the forcing frequency.

6. Acknowledgements

We are grateful for the support provided by the Air Force Office of Scientific Research through contract F49620-98-1-0276. The program was managed by Dr. Steven Walker. NASA Space Grant provided partial support for D. Williams. A special thanks goes to Mr. Ken Ostasiewski, Mr. Tim Hayden and SSgt. Buddy Johns for their patience and assistance during the experiments.

7. References

1. Krishnamurty, K., "Acoustic radiation from two-dimensional rectangular cutouts in aerodynamic surfaces" N.A.C.A. Tech. Note 3487, August, 1955.
2. Roshko, A., "Some Measurements of Flow in a Rectangular Cutout," N.A.C.A. Tech. Note 3488, August, 1955.
3. McGregor, O.W., and White, R. A., "Drag of Rectangular Cavities in Supersonic and Transonic Flow Including the Effects of Cavity Resonance," AIAA J., **8**, 1970.
4. Pinney, M. A., and Leugers, J. E., "Experimental Investigation of the Impact of Internal/External Weapons carriage on a Generic Aircraft configuration," WL-TR-96-3110, Final Report, Wright Laboratory, 1996.
5. McGrath, S. and Shaw, L., "Active Control of shallow cavity acoustic resonance," AIAA paper 96-1949, 27th AIAA Fluid Dynamics conference, New Orleans, June 1996
6. Colonius, T., "An Overview of Simulation, Modeling and Active Control of Flow/Acoustic Resonance in Open Cavities," AIAA Paper 2001-0076, 39th AIAA Aerospace Sciences Meeting & Exhibit, Reno NV, Jan 2001.
7. Grove, J. E., Pinney, M.A., Stanek, M.J., "A Cooperative Response to Future Weapons Integration Needs," Symposium on Aircraft Weapon System Compatibility and Integration, Chester UK, Sept. 1998, pp.24-1 24-12.
8. Shaw, L. and Northcraft, S., "Closed Loop Active Control for Cavity Acoustics," AIAA Paper 99-1902, June 1999.
9. Cattafesta, L.N. III, Garg, S., Choudhari, M., Li, F., "Active Control of Flow-Induced Cavity Resonance," AIAA 97-1804, 28th Fluid Dynamics Conf. Snowmass Village CO, 1997.
10. Raman, G., Envia, E., Bencic, T., "Tone Noise and Nearfield Pressure Produced by Jet-Cavity Interaction," AIAA paper 99-0604, 37th Aerospace Sciences Meeting, Reno NV, 1999.
11. Fabris, D. and Williams, D.R., "Experimental Measurements of Cavity and Shear Layer Response to Unsteady Bleed Forcing," AIAA paper 99-0605, 37th Aerospace Sciences Meeting, Reno NV, 1999.
12. Cattafesta, L. N. III, Garg, S., Kegerise, M.S., Jones, G.S., "Experiments on Compressible Flow-Induced Cavity Oscillations," AIAA-98-2912, 1998.

13. Williams, D. R., Fabris, D., Iwanski, K., Morrow, J., "Closed loop control in cavities with unsteady bleed forcing," AIAA Paper 2000-0470, 38th Aerospace Sciences Meeting and Exhibit, Reno NV, January 2000.
14. Rossiter, J.E., "Wind-Tunnel Experiments on the Flow over Rectangular Cavities at Subsonic and Transonic Speeds." Aeronautical Research Council Reports and Memo No. 3438, 1966.
15. Kegerise, M. A., "An Experimental Investigation of Flow-Induced Cavity Oscillations," Ph.D. Dissertation, Syracuse University, 1999.
16. Dix, R.E. & Bauer, R.C., "Experimental and Predicted Acoustic Amplitudes in a Rectangular Cavity," AIAA Paper 2000-0472, 38th Aerospace Sciences Meeting & Exhibit, Reno NV, Jan. 2000.
17. Bilanin, A.J., and Covert, E.E., "Estimation of possible excitation frequencies for shallow rectangular cavities," *AIAA J.*, **11**, 1973.
18. Tam, C.K.W., and Block, P.J.W., "On the tones and pressure oscillations induced by flow over rectangular cavities," *J. Fluid Mech.*, **89**, part 2, 1978.
19. Sarohia, V., "Experimental and analytical investigation of oscillations inflows over cavities," Ph.D. Thesis, California Institute of Technology, 1975.
20. Hankey, W.L., and Shang, J.S., "Analyses of Pressure Oscillations in an Open Cavity," *AIAA J.* **18**, No. 8, 1980.
21. Cain, A.B., Bower, W.W., McCotter, F., and Romer, W.W., "Modeling and Prediction of Weapons Bay Acoustic Amplitude and Frequency," Aerospace Report Number MDA 96X0009, Final Report under P.O. P61100-5016, submitted to VEDA Inc., February 1996.
22. Rowley, C.W., Williams, D.R., Colonius, T., Murray, R.M., MacMartin, D.G., Fabris, D., "Model-Based Control of Cavity Oscillations, Part II: System Identification and Analysis," AIAA Paper 2002-0972, 40th Aerospace Sciences Meeting & Exhibit, Reno NV, Jan. 2002.
23. Snyder, S.D. "The Active Noise Control Primer," Arbor Scientific, 1997.
24. Pillarisetti, A., Cattafesta, L.N., Kurdila, A.J., "Adaptive Identification of Fluid-Dynamic Systems," 31st AIAA Fluid Dynamics Conference & Exhibit, Anaheim, CA.
25. Cattafesta, L.N., Shukla, D., Garg S., Ross, J.A., "Development of an adaptive weapons-bay suppression system," AIAA Paper 99-1901, May 1999.
26. Williams, D.R., Fabris, D., Morrow, J., "Experiments on controlling multiple acoustic modes in cavities," AIAA Paper 2000-1903, 6th Aeroacoustics Conf. June 2000.
27. Rockwell, D. & Naudascher, E., "Self-Sustaining Oscillations of Impinging Free shear Layers," *Annual Review of Fluid Mechanics*, **11**, pp67-94, 1979.
28. Oster, D. and Wygnanski, I., "The Forced Mixing Layer Between Parallel Streams," *J. Fluid Mech.* **123**, pp 91-130, 1982.

8. Figures

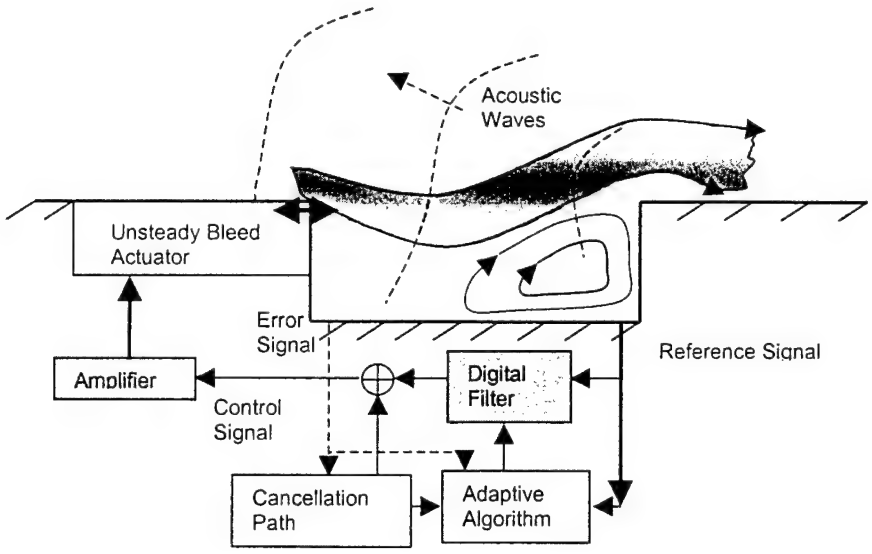

Fig. 1 - Block diagram of adaptive feed-forward control algorithm.

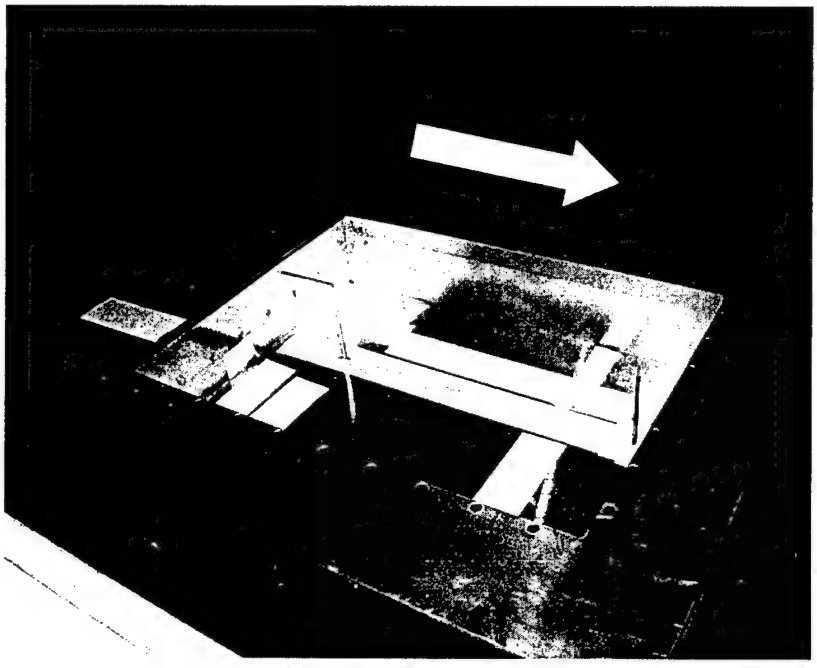

Fig. 2 – Photograph of cavity in Subsonic Wind tunnel and hot film probes at upstream and downstream locations.

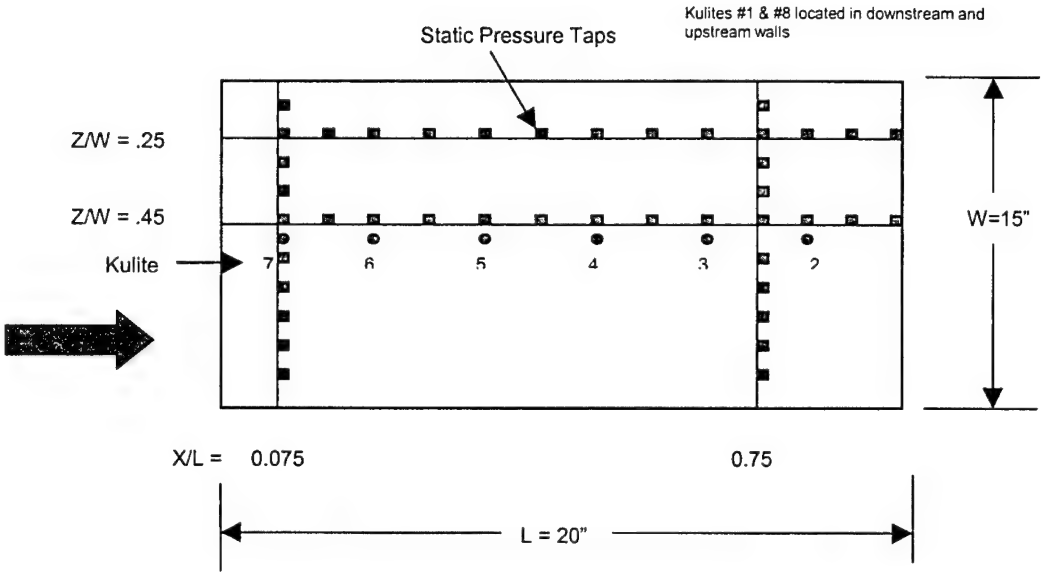

Fig. 3 - Static pressure tap and Kulite sensor locations. The cavity was instrumented with eight Kulite sensors (model XCS-093) positioned from the front wall to the rear wall along the centerline of the cavity.

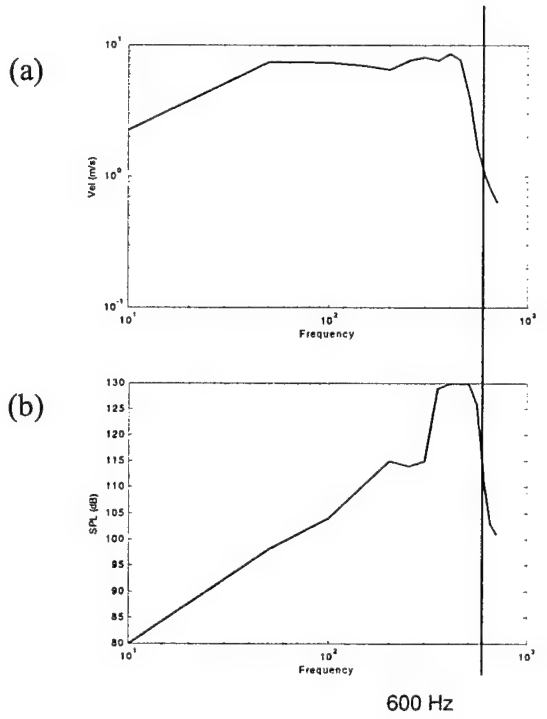

Fig. 4 – The response functions of the actuator are reproduced in Fig. 4 from Ref.[16].

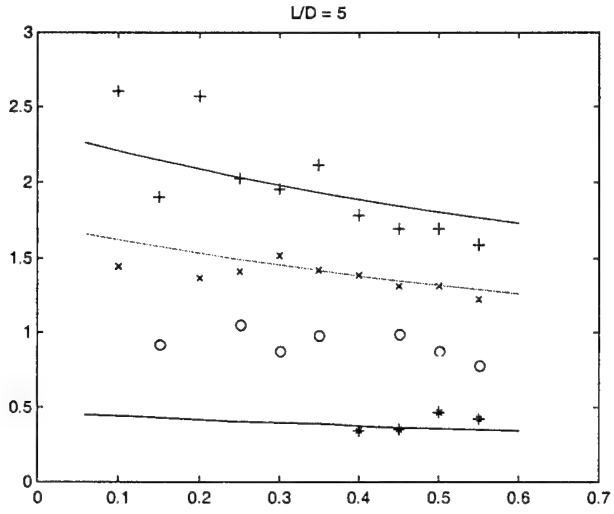

Fig. 5 – Rossiter diagram of first four resonant modes vs. Mach number.

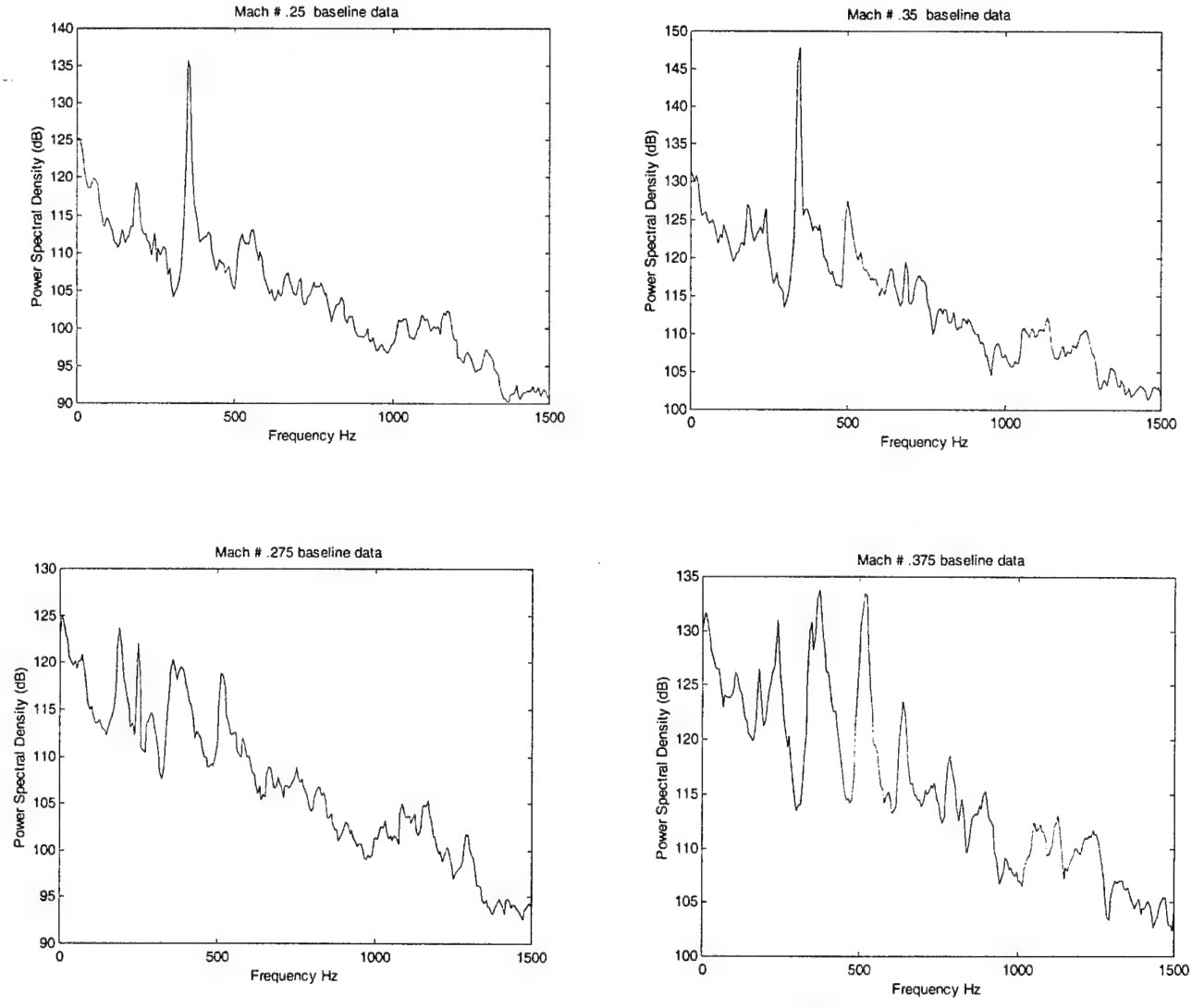

Fig. 6 - Spectra showing single and multimode resonance. a) & d) Single mode resonance; b) & d) multimode resonance.

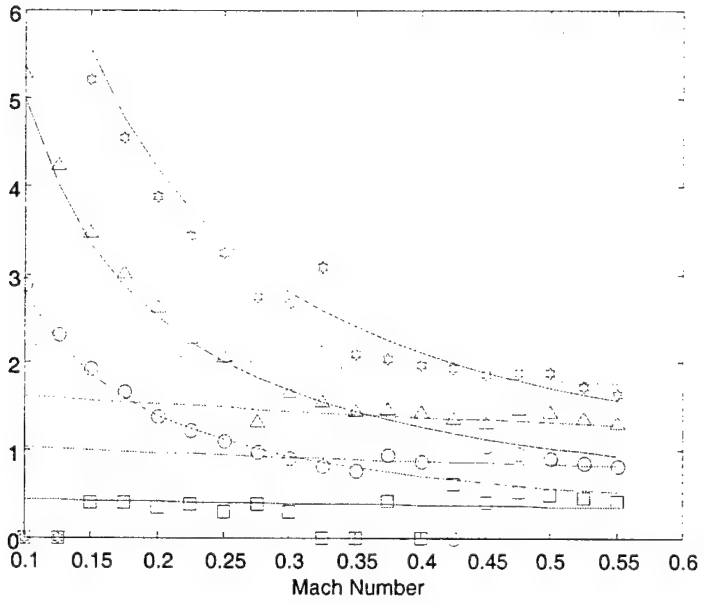

Fig. 7 - Superposition of the normal cavity modes with Rossiter modes. The intersection of the first longitudinal mode with the Rossiter modes coincides with the Mach number of single-mode resonance.

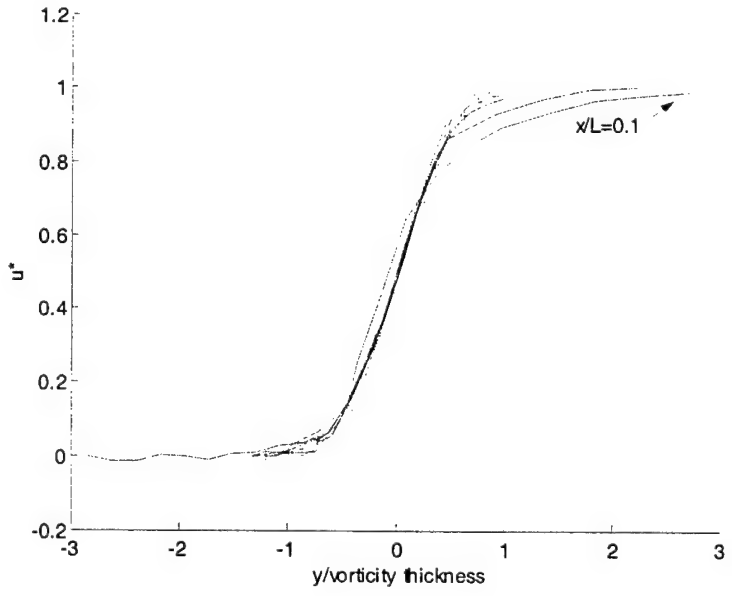

Fig. 8 – Normalized mean velocity profiles from x/L = 0.1 to x/L = 0.6, M = 0.35. The y-coordinate is normalized by the vorticity thickness. The normalized velocity is $u^* = (U(y)-U_1)/(U_2 - U_1)$.

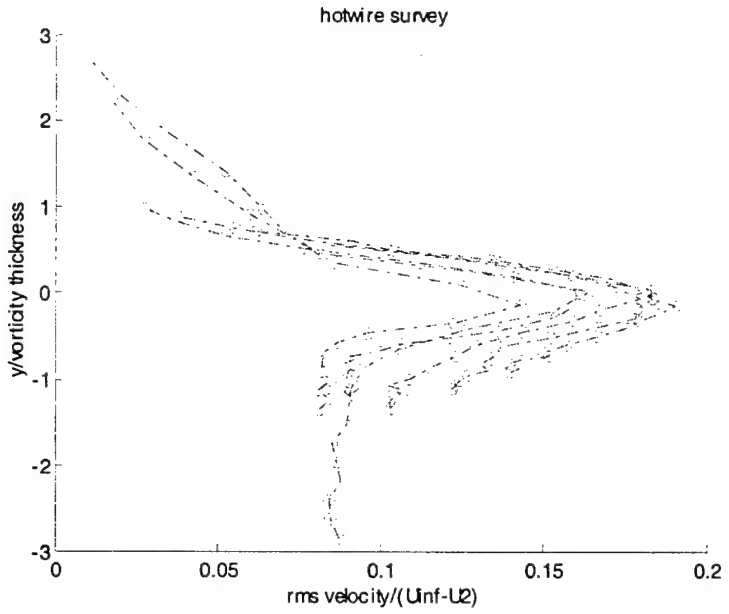

Fig. 8b - Fluctuating velocity profiles with the y-coordinate normalized by the vorticity thickness.

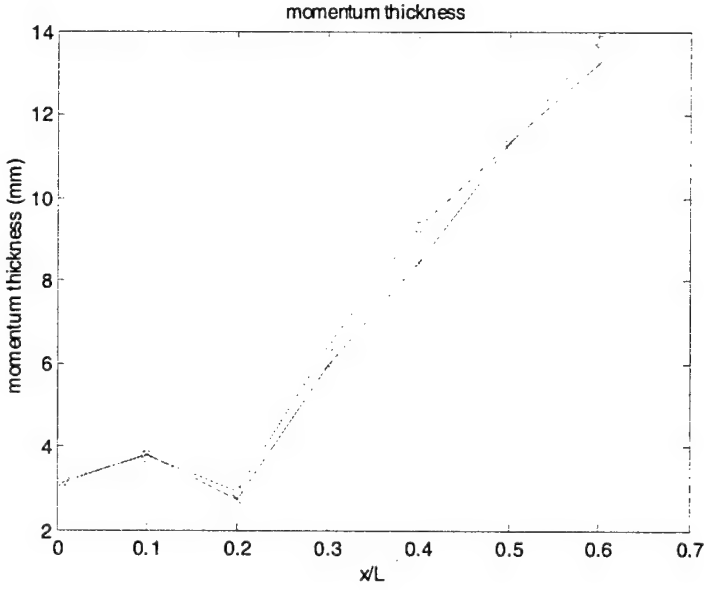

Fig. 9 - Shear layer momentum thickness growth with and without forcing.

(a)

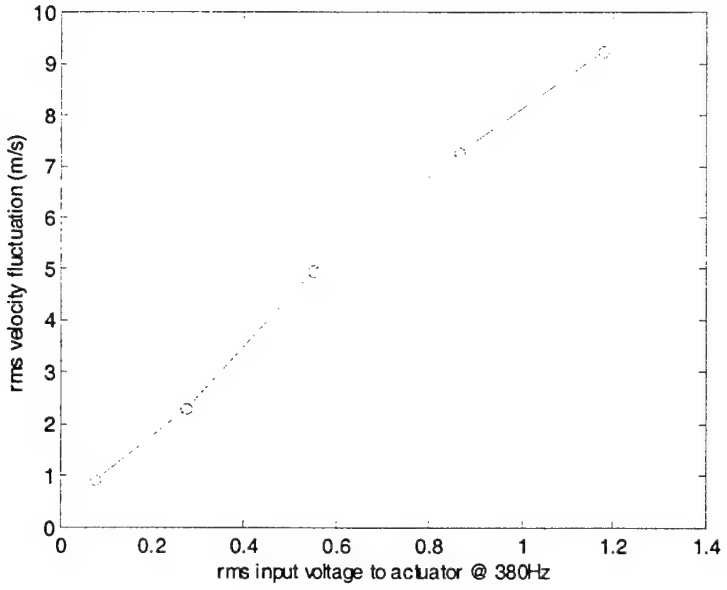

(b)

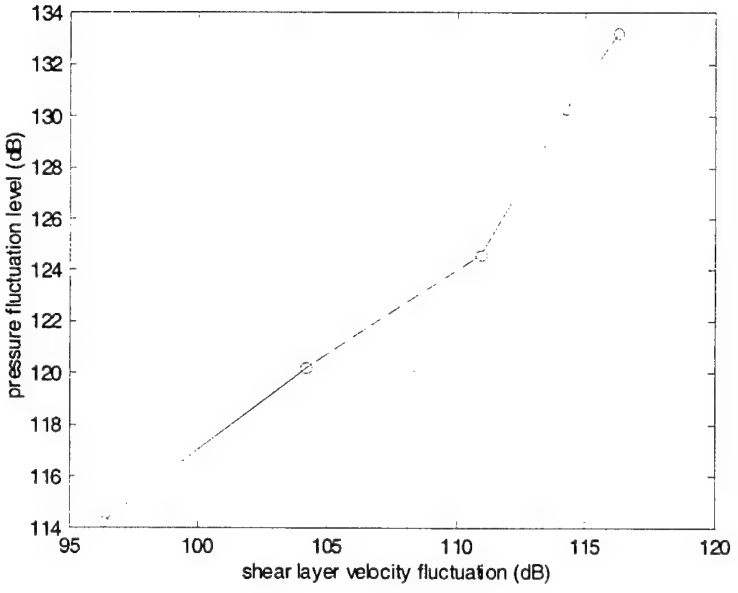

Fig. 10 – (a) Dependence of shear layer velocity fluctuation amplitude on voltage input to the actuator. (b) Sound pressure level in cavity at 380 Hz dependence on initial shear layer velocity fluctuation amplitude.

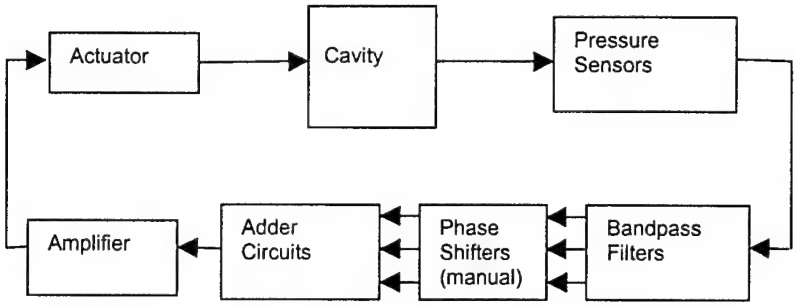

Fig. 11 – Block diagram of analog control system.

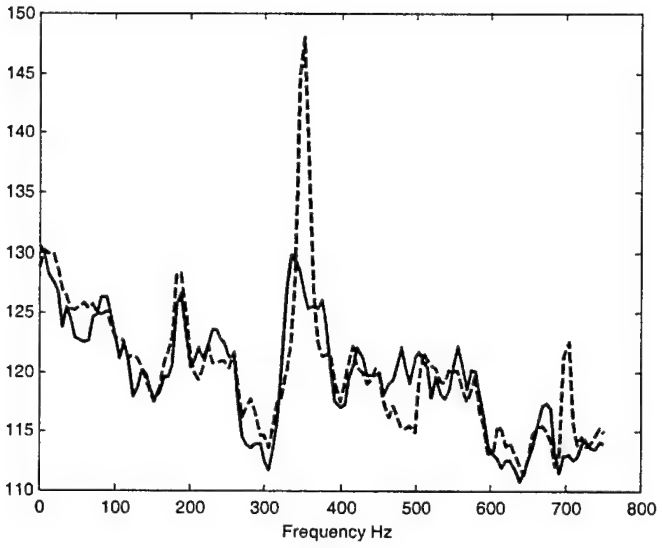

Fig. 12 - Single-mode suppression at M = 0.34 with the analog controller. The dotted line corresponds to the baseline case.

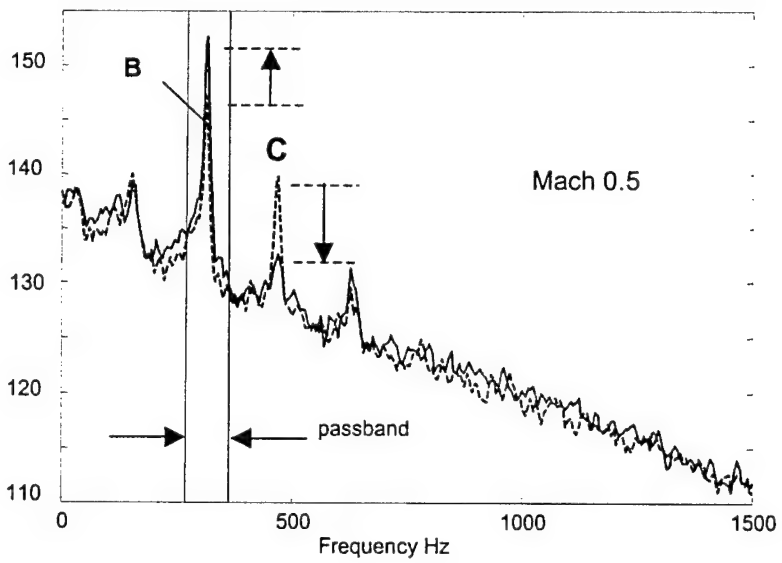

Fig. 13 - Enhancement of second Rossiter mode 'B' suppresses energy in third Rossiter mode 'C'. The dashed line shows the uncontrolled baseline spectrum.

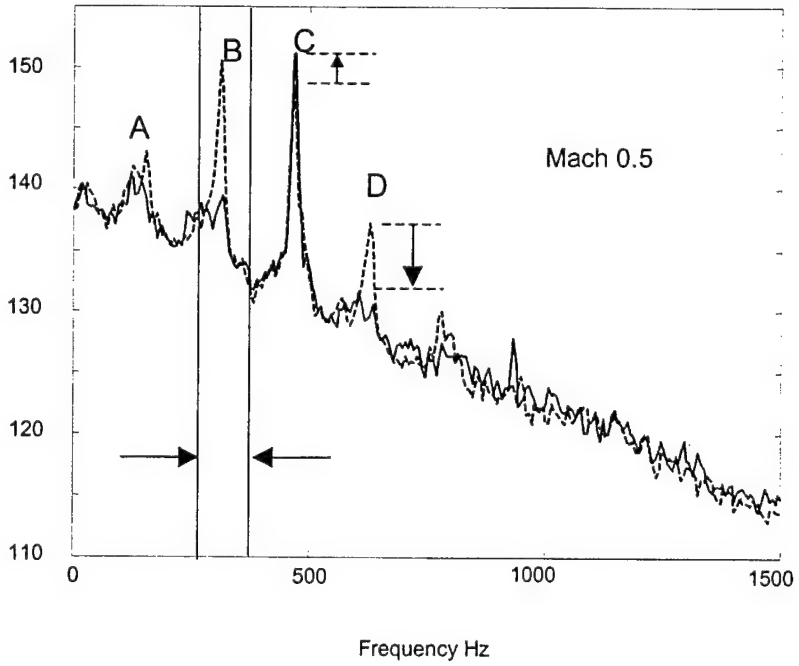

Fig. 14 - Suppression of second Rossiter mode 'B' enhances energy in third Rossiter mode 'C' and suppresses the fourth mode 'D'. The dashed line shows the uncontrolled baseline spectrum.

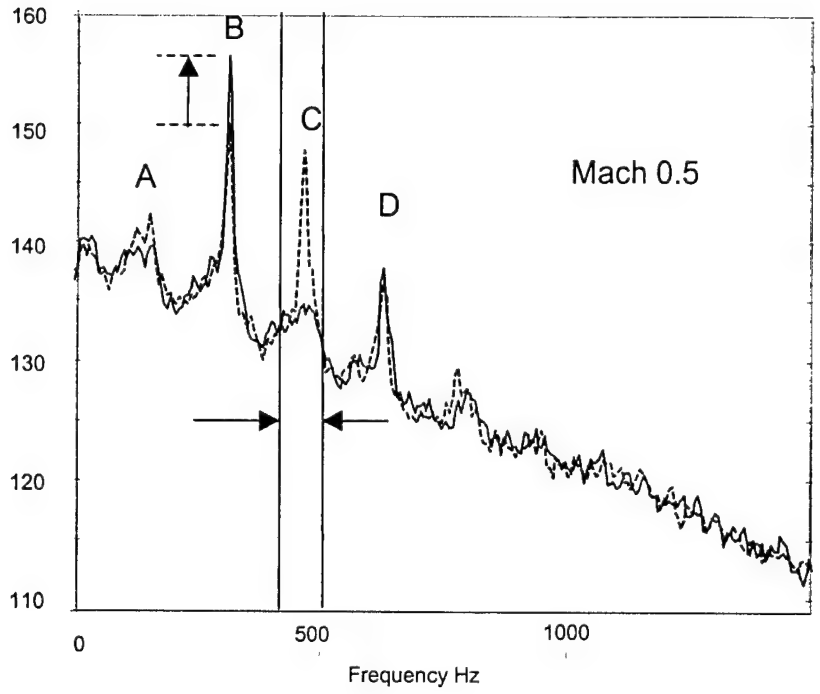

Fig. 15 – Suppression of third Rossiter mode (C) enhances energy in second Rossiter mode and slightly suppresses the first mode. This establishes a connection between odd modes. The dashed line shows the uncontrolled baseline spectrum.

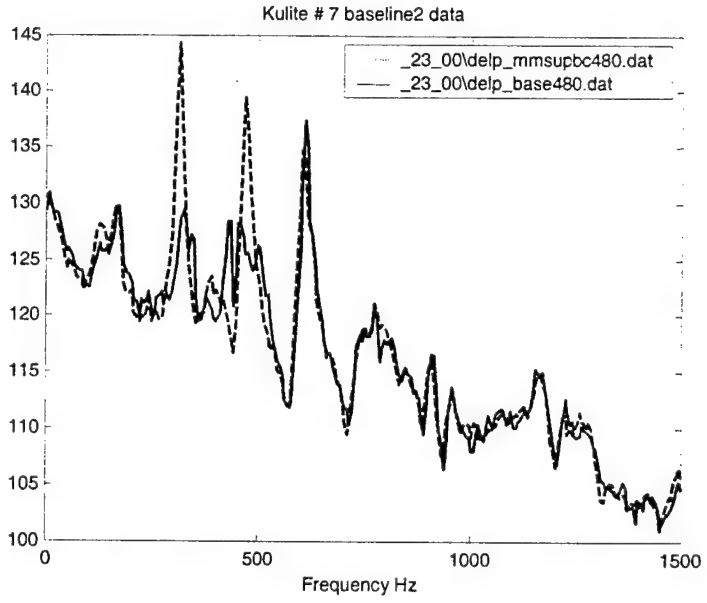

Fig. 16 - Multimode suppression of Rossiter modes B and C by 15dB and 13 dB, respectively. M = 0.48

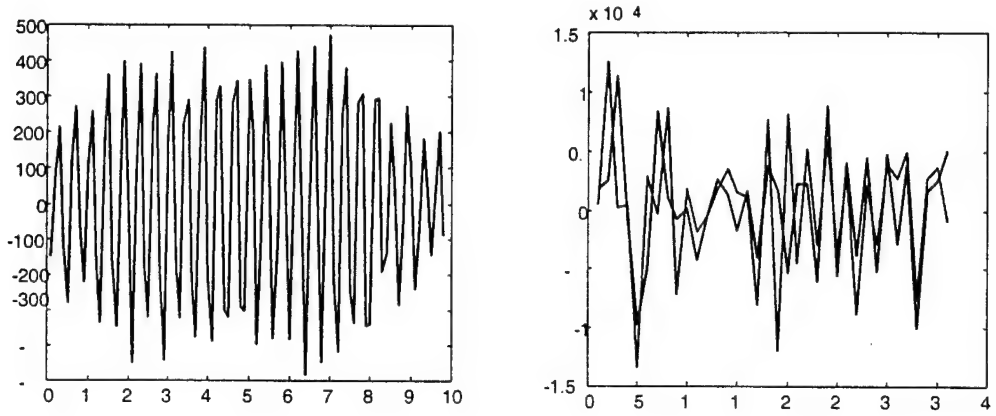

Fig. 17 - Cancellation path model and complex control filter coefficients for M = 0.35.

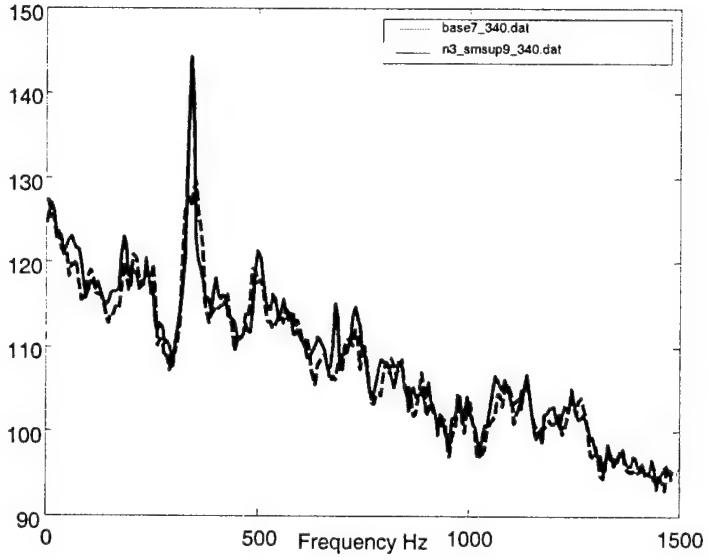

Fig. 18 - Spectrum at M = 0.34 digital control suppression of 15 dB at 341 Hz. The spectra compare the error sensor signals obtained from Kulite 7 located near the upstream wall of the cavity.

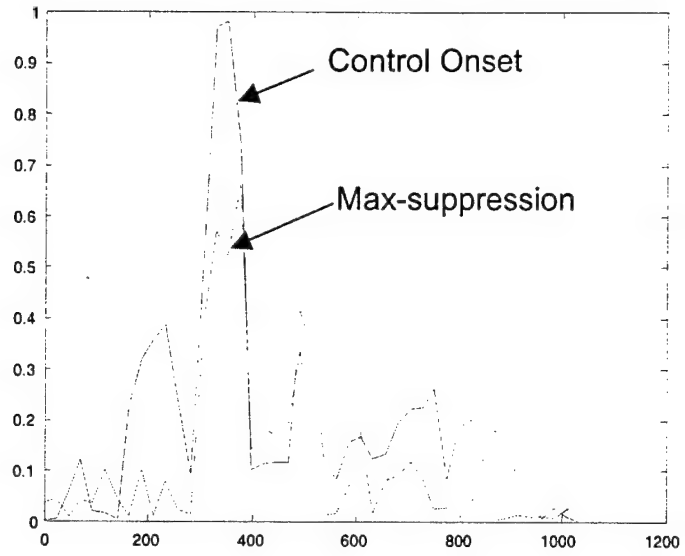

Fig. 19 - Comparison of coherence with at onset of control and at maximum suppression of a single mode at M = 0.34.

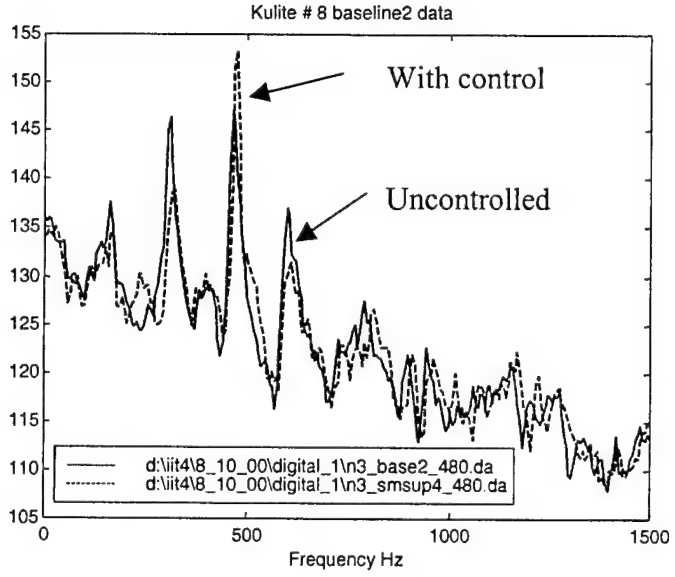

Fig. 20 - Multimode suppression with the digital controller at M = 0.48. Energy shifts to the third Rossiter mode when the second and fourth modes are suppressed.

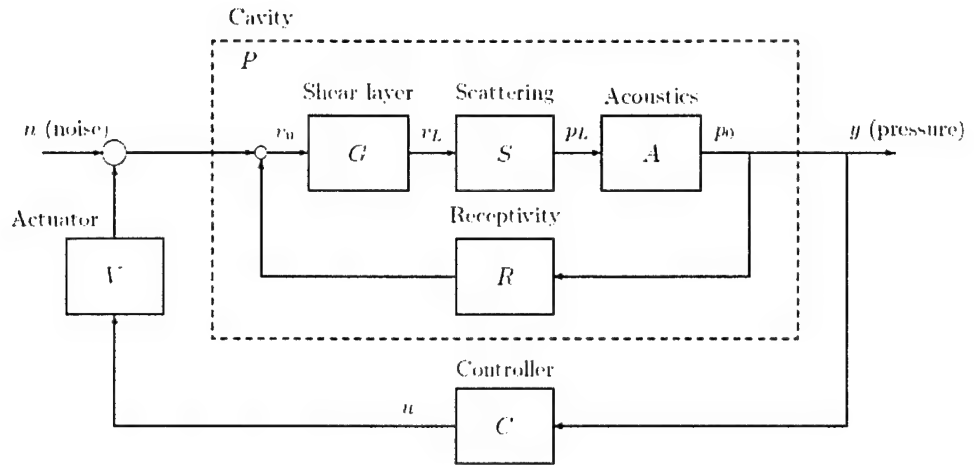

Fig. 21 – Block diagram of Rowley, et al.[22] flow physics model. Figure reproduced from Ref [22].

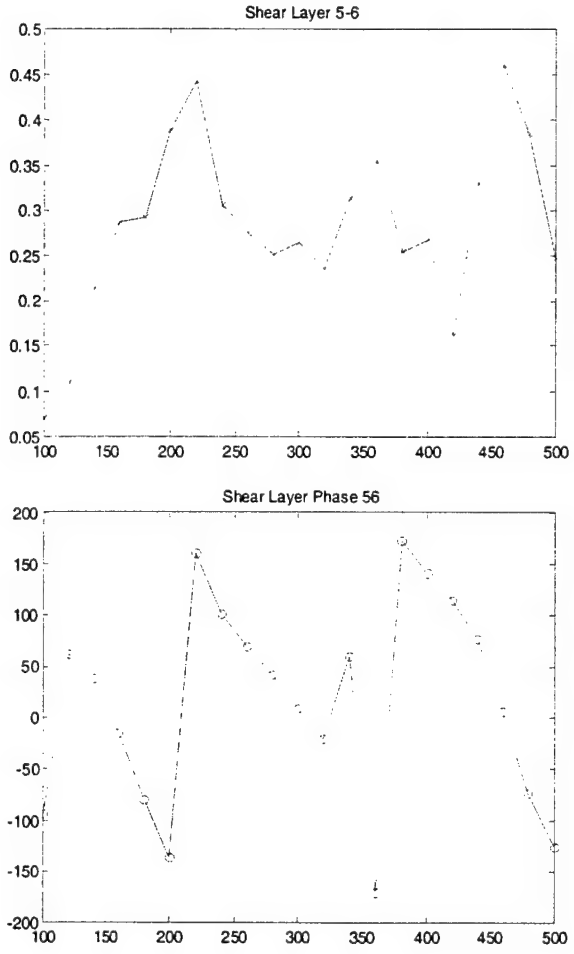

Fig. 22 - Shear layer transfer function with phase obtained with open loop forcing. (a) transfer function; (b) phase.

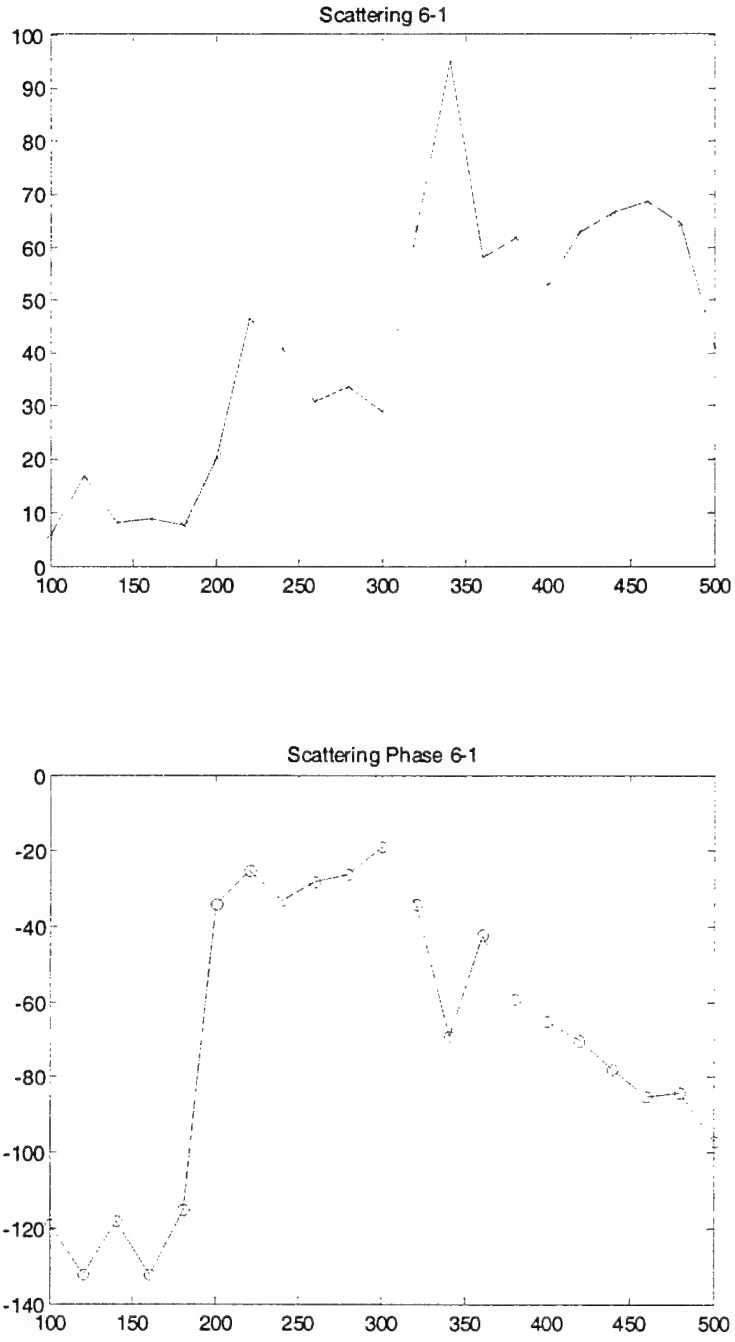

Fig. 23 - Scattering transfer function with phase obtained with open loop forcing between the downstream hot film probe and pressure transducer in downstream wall. (a) transfer function; (b) phase.

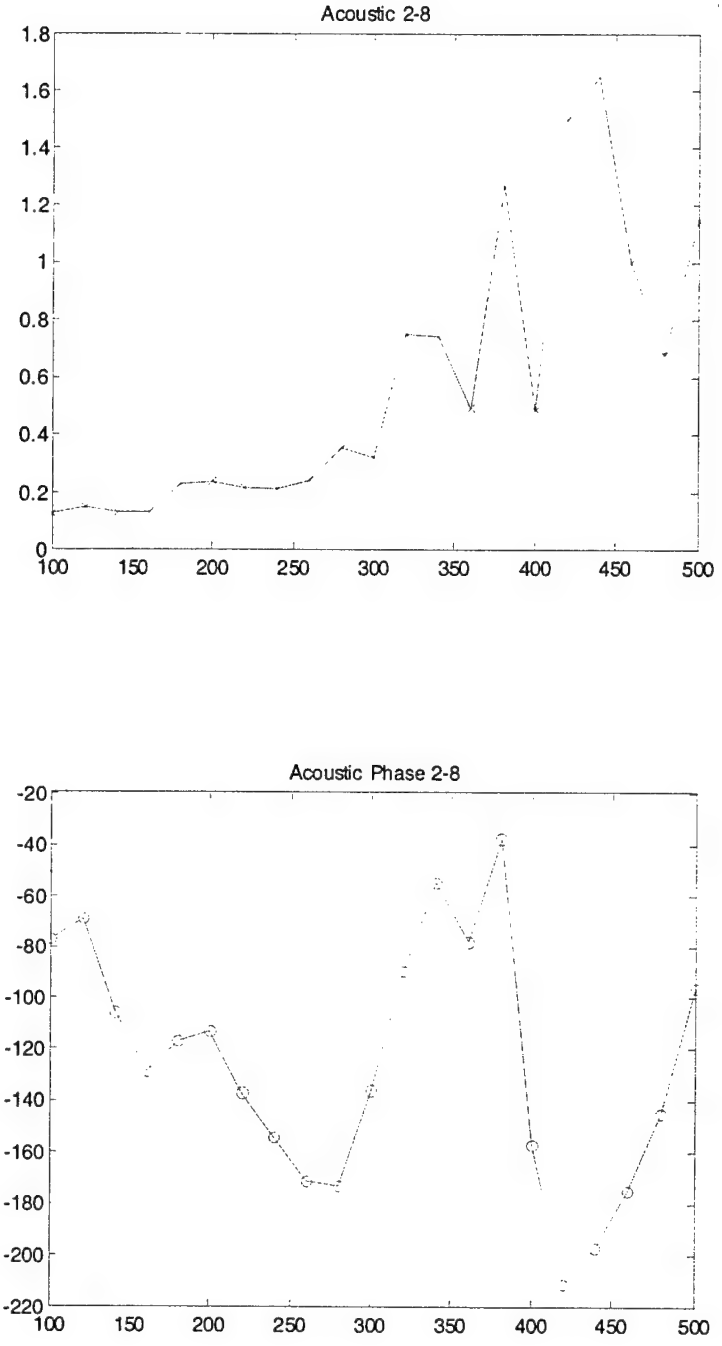

Fig. 24 - Transfer function of upstream propagating acoustic wave.

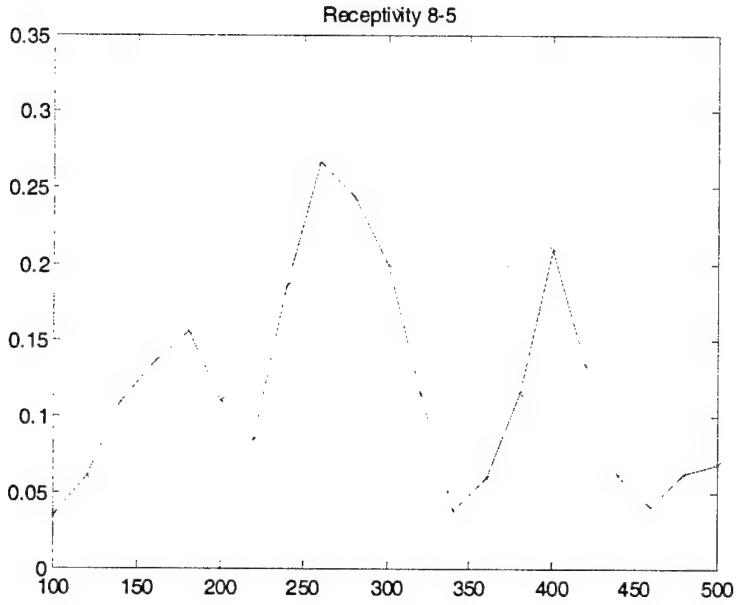

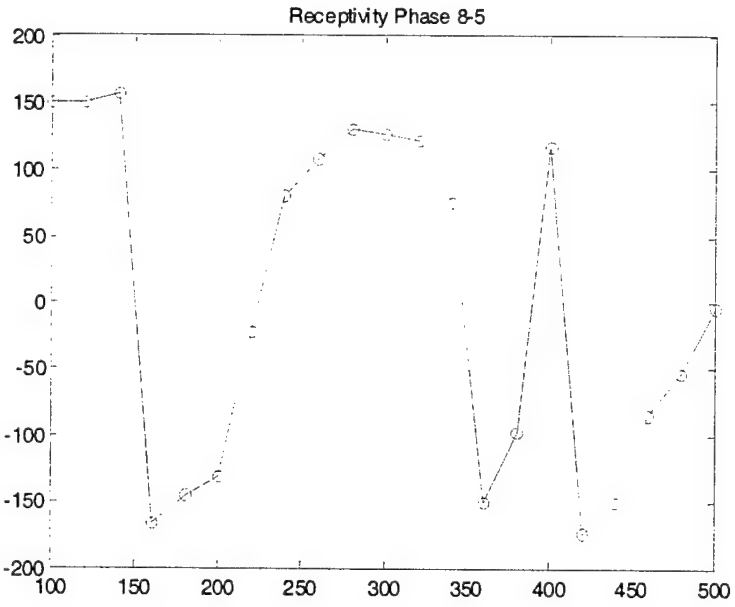

Fig. 25 - Leading edge receptivity measured between pressure transducer in the upstream wall and a hot-film probe located in the shear layer. (a) transfer function; (b) phase.

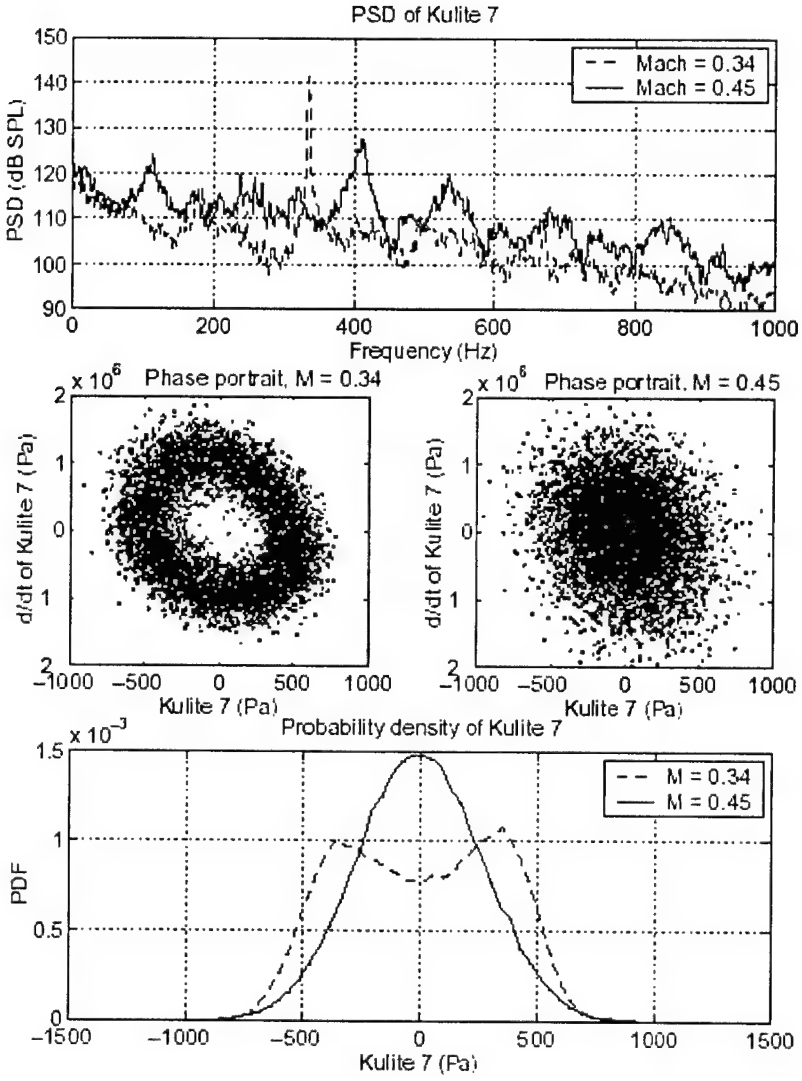

Fig. 26 – (from Rowley, et al.[22]) – Spectra, phase plots and probability density plots corresponding to self-excited and modes at M = 0.35 and 0.45, respectively. The M= 0.34 mode is self-excited, while the M=0.45 case is driven by noise.

9. Appendix

– Synopsis of Experiments at USAFA 1999 – 2001

1. First entry – baseline studies, open-loop and preliminary closed-loop control experiments

USAFA cadets Himsl (et al) conducted the preliminary experiments during the spring semester in 1999. Pitot tube surveys of the boundary layer and Kulite pressure sensor measurements of the noise levels were done. (Reference their report.) The initial results indicated possible tunnel mode acoustic modes were present, which could contaminate the cavity data. Acoustic foam was added to the ceiling of the wind tunnel to damp these modes. All experiments in the preliminary test phase were done without control.

May 17, 1999 (Monday)
Installed forcing system and acoustic foam
Nozzle #1 has 0.25 inch slot height, and was used for all of the tests in May.

May 18, 1999 (Tuesday)
L/D =
Horizontal nozzle installed on forcing system.
Installed Kulites and static pressure taps
Baseline flow measurements M = 0.1, .2, .3, .4, .5, .55
Open loop forcing experiments at M = 0., 0.1, 0.2, 0.3, 0.4 … determined that speaker was being sucked into the tunnel. Designed and constructed a box housing for the speakers.

May 19, 1999 (Wednesday)
L/D =
Horizontal nozzle used.
Open loop forcing experiments M = 0.1, .2, .3, .4, .5
Feedback control experiment with one microphone M = 0.3.
Lab photos taken.
Change to 45o nozzle and do closed-loop forcing at M = 0.3
Change to 90o (vertical) nozzle and do closed-loop forcing

May 20, 1999 (Thursday)
Change back to horizontal nozzle for baseline2 data
Vary cavity depth: "a" L/D =5; "b" L/D = 4; "c" L/D = 2
Baseline tests (no forcing) done for M = 0.1 – 0.55 with L/D = 4
Baseline tests (no forcing) done for M = 0.1 – 0.55 with L/D = 5
Baseline tests (no forcing) done for M = 0.1 – 0.55 with L/D = 2
Closed-loop control L/D = 2, M = 0.35
Closed-loop control L/D = 4, M = 0.30
Repeat of baseline data with L/D = 4

May 21, 1999 (Friday)

Closed loop forcing with L/D = 4, M = 0.30; Changing amplifier gain systematically
Closed loop forcing with L/D = 4, M = 0.30; Changing phase systematically
Rewired loudspeaker system so speakers were out-of-phase with each other and checked performance with M = 0.30 closed-loop feedback control.
Attempt to control multiple modes near M = 0.35, 0.475, 0.47, 0.325
Closed loop forcing with L/D = 5, M = 0.3, 0.32
Multiple mode control at M = 0.32
Very "pure" resonance observed at M =0.34.
Changed Kulite arrangement to be spanwise across the floor of the cavity
Baseline (no forcing data) obtained at M = 0.1, 0.2, 0.3, 0.4

2nd Entry

August 3, 1999 (Tuesday)
Kulites aligned in the flow direction along the floor of the L/D=5 cavity and calibrated.
Different nozzles were built for the actuator, which had different opening sizes.
Baseline L/D = 5, M = 0, .125, .225, .275, .325, … ,0.525, and repeated.
Single mode suppression with closed loop control with nozzle 1, L/D = 5, M = .325, .35, .4, .475, .5, .525
Multiple mode suppression – suppress individual modes first independently then in combination at M = 0.5. Cancellation of one mode led to enhancement of the other mode.

August 4, 1999 (Wednesday)
Multiple mode suppression experiments L/D = 5, M = 0.5
Transient response to turning on/off different bandpass filters
Changing nozzle width experiments, Nozzle #2 with 1/8" gap, L/D = 5, M = .35, .525
Nozzle #3 with ½" gap, M = .35, .5, .525 and repeated experiments
Nozzle #4 with 1" gap, M = .35, .5, .525, L/D = 5
Change to deeper cavity with L/D =4, nozzle #4, M = .25, .3, .45, .525, .5
Nozzle #3 L/D = 4 M = .3, .45, .525, .5
Nozzle #2 L/D = 4 M = .3, .45, .525, .5

August 5, 1999 (Thursday)
Single mode suppression and transient experiments
Nozzle #2 L/D = 2 M = .25, .3, .45, .5
Nozzle #4 L/D = 2 M = .25, .3, .45, .5
Nozzle #3 L/D = 2 M = .25, .3, .45, .5----last of nozzle variation tests
Transient control of single modes with nozzle #3 (1/2" gap), L/D = 5, M = 0.35, .5, .525
Single speaker control tests M = .35, .475, .5 yielded smaller amounts of control.
Two speaker control with Nozzle 4, 1" gap, M = .525, .5, .475, .35- single mode and transient cases studied
Nozzle #1 (¼" gap) M = .525, .48 (three modes observed), .35, .325
Files of particular importance showing energy switch of 5-10dB among all 4 modes, see n3r_mmabsup500, n2r_mmabsup525, n4_mmabsup500 and n4_mmsup500a2.

August 6, 1999 (Friday)

Attempt to ramp up freestream Mach number from 0.3 – 0.35, nozzle 3, L/D = 5
Multimode suppression experiments with nozzle 3, M = .48, started with single mode suppression of individual frequencies within the multimode spectrum.
Successful multimode suppression experiments were achieved in this data set.
MSI piezoelectric plate installed and tested.
Deep cavity L/D = 2 experiments with nozzle 4- M = .25, .3, .325, .35, .275, .225
Boeing tests with Wygnanski strings on cavity.

3rd Entry
May 15, 2000 (Monday)
Setup equipment for cavity with nozzle 3, L/D = 5 for active noise control experiments.

May 16, 2000 (Tuesday)
No flow calibrations of Kulite sensors.
Kulite #8 used for feedback control experiments set up.

May 17, 2000 (Wednesday)
Test of hotwire anemometer and stepper motor system
Background noise tests with loudspeaker only, 100Hz – 1000Hz, 1Vpp input from function generator
Single mode control case at M = .35
Multi mode control case M = .48
Various filter settings and combinations of mode suppressions, however, difficulty in achieving significant mode suppression.
*Calibration of Phase Shift Circuit

May 18, 2000 (Thursday)
Changed speaker polarity and attempted additional multi-mode experiments. Not successful
Pitot survey of boundary layer profiles, M = .25 - .55

May 19, 2000 (Friday)
Install hot wire anemometer on traverse.

May 22, 2000 (Monday)
Calibration of hot wire in tunnel freestream
*Characterize forcing out of actuator. Hot wire traverse of actuator slot exit of nozzle 3. Complete y-traverse distance is ½", +/- ¼" above and below the nozzle. Actuator forced at 1Vpp with frequencies of 10Hz – 700 Hz.
*Phase between velocity fluctuations at slot exit and Kulite signals with no flow in tunnel measured at frequencies from 10Hz to 700 Hz. Hotwire fixed at center of nozzle slot.
Experiments to see if suppression of resonance produces a detectable change in tunnel static pressure drop across the cavity.
Calibration of Kulites with B&K calibrator.
Change feedback signal to Kulite 7. Added additional preamplifier to feedback signal circuit, which greatly improved the performance of the control system.
Calibrated hot wire again.

May 23, 2000 (Tuesday)
Calibrated hot wire.
Using Kulite 8 as the feedback signal, attempted to measure static pressure change in tunnel with and without suppression. M = 0.25 – 0.48. Some good multi-mode suppression cases were obtained in this dataset.

Hot wire traverse of shear layer at different downstream locations, M = .35, .48 with and without control. L = 20"
X locations = 1/8", 2", 4", 6", 8", 10", 12"

May 24, 2000 (Wednesday)
Complete hot-wire surveys of shear layer.
Flow control experiments using the hot-wire signal as the feedback, M = .25, 0.3, .35. Hot wire probe was located at 1.5" above edge of cavity and at x/L = 0.3.
*Hot wire signal recorded on channel 7 with very small changes in Mach number (.125), and the Mach number was varied from .1 - .55. Objective is to confirm single-mode character of the resonance at specific values of the Mach number.

May 25, 2000 (Thursday)
Open loop forcing experiments with the hot wire located at x/L = 0.3, y = 1.5" above cavity lip. Objective is to determine transfer function of actuator. M = .35, .25, .48 and .35. Excitation frequencies 100Hz – 700Hz, and excitation amplitudes 1Vpp(?), 2Vpp, and 3Vpp.
*Measurement of phase across the shear layer at M = .35, x/L = 3. Phase reference is Kulite #8, and hot wire signal is on channel 7. Hotwire coupled directly to ADC without filtering.
Hot wire control experiment at M = .35.
Hot wire calibration
Multi-mode control experiments using 3 feedback bands at M = .5, .48, .4, .375, .35, .3, .25.

<u>4th Entry</u>
August 7, 2000 (Monday)
Measurements of test section pressure drop without the cavity installed, i.e. flat plate.
Install cavity and actuator.

August 8, 2000 (Tuesday)
Calibration of actuator and data acquisition system using open loop forcing, no flow, 1Vpp, frequencies from 100Hz – 1000Hz. Repeat with 5 Vpp.
Closed-loop control tests with the modified 8"loudspeaker actuator. The interior divider section was removed from the actuator after the previous entry into the wind tunnel. Initial attempt was to suppress one mode at a time in the multi-mode resonance case at M = 0.48.

August 9, 2000 (Wednesday)
*Closed-loop control experiments at M = .34. Both enhancement and suppression were demonstrated.

Digital control setup with the commercial adaptive noise control system. Kulite 8 used as reference signal and Kulite 4 the error signal, M = 0.34. System was successful in reducing single peak in spectrum.

August 10, 2000 (Thursday)
Digital control experiments conducted with Kulite 4 as the error signal and Kulite 7 as the reference signal. There was concern that Kulite 8 may see too much of the actuator signal through wall vibration. Single mode suppression experiments at M = 0.48, .34.
Experiments with FIR vs IIR filters. In general IIR filters perform better and with fewer coefficients, so long as they do not go unstable.
Analog phase shift circuit added to output of control signal.
Experiments conducted with changing the reference signal to different Kulites 2, 3 to see the effect of physical location.
Analog control experiment done at M = .34 to be used as comparison case with digital control.
Calibration check of Kulites using B&K calibrator
Effects of convergence coefficients, cancellation path, digital filter length and leakage factors studied. Kulite 3 used as reference signal and Kulite 7 is error signal. Experiments were done at M = .34, .35.
Installed new actuator that uses 5" diameter speakers.

August 11, 2000 (Friday)
Calibration of 5" actuator system. Speaker system was damaged while running at M = .48.
Reinstall 8" speaker system.

August 14, 2000 (Monday)
Kulite 3 (reference) and Kulite 7 (error) signals bandpass filtered through Ithacos before used as input to digital controller. M = 0.48, .25, .35, .375. Various types of filters, convergence coefficients were used with digital controller.
*File n3_smsup3_350 produced strong reduction (18dB at fundamental) but enhanced a new mode at 500Hz. Could be a first example of peaking.
Comparisons of IIR vs. FIR filtering were made at M = .34

August 15, 2000 (Tuesday)
Digital control at M = .25, .525 compared with analog controller. Additional peaks appeared in spectrum once fundamental was suppressed in M = .525 case.
M = .475, .375, .35 multi-mode cases studied.
Effect of decreasing convergence coefficient studied at M = .4, .35.

August 16, 2000 (Wednesday)
Checks of the external signals produced by the commercial control system package.
Calibration shows that the 95dB peak in the channel 4 control signal used on 8_15_00/n3_smsup8_350 file corresponds to a 0.014V output from the DSP. This may explain the limited dB reduction seen in the frequency to be controlled.
Digital closed-loop control using narrow band filters to allow for larger input signal amplitudes. These gave greater reductions but produced sidebands. (n3_smsup_350)
Experiments conducted with larger numbers of filter taps.

Mean tunnel pressures recorded in "pressure" folder at M = 0.35.
Multimode suppression experiments at M = 0.375, .48. Receptivity at leading edge was to be determined from interior pressures and hot wire signal.

August 17, 2000 (Thursday)
Hot wire probe placed 1/8" downstream of cavity lip at y=0.
M = .35, M =0.48 transient cases with controller.
Hot wire moved to ¼" downstream. M = .35, .48 with some transient cases.
Hot wire moved to x/L = 0.044. M = .35, .48
Hot wire moved to x/L = .094, .144, .344 and M = .35, .48.
Calibration of hot wire.
Pressures inside cavity measured with control on and off for M = .25, .3, .325, .35, .4, .45, .48.

August 18, 2000 (Friday)
Hot wire calibration of velocities from the actuator. Hot wire placed in middle of slot.
Kulites 2,3,4,5,6,7 reversed in their order on the floor to provide independent check of calibration accuracy.

5. Closed-Loop Control using dSPACE control system and flow phsics based algorithm
June 18, 2001 (Monday)
Nozzle used has gap height of 3/16."
Set up equipment and install electromagnetic wire-type actuator.
Measurements of electronic noise levels through analog Butterworth filter circuits.
Open loop forcing experiments with wire actuators, M = 0.1, .15, ..., .45. Wire broke during M =.35 data set. Wires vibrated at flow-induced vibration frequency, but were capable of producing an independent control signal.
Install loudspeaker type actuator.

June 19, 2001 (Tuesday)
Set up analog control system for M = .34 experiments.
Set up dSPACE control system.
Test of "filtergainphase" digital control algorithm, which simulates analog control.
Proof-of-concept experiment to suppress Rossiter modes, then superpose open-loop mode on top. 200 Hz wave added to suppressed flow at M =.34.

*Interesting observation on the oscilloscope that Kulite 8 signal compared with the control signal to power amp (channel 4) rapidly jumped back and forth from being in-phase to some other out-of-phase state near 180o. The implication was that the controller locks on to itself part of the time.

June 20, 2001 (Wednesday)
Transfer function of anti-aliasing filter measured.
Two hot-film probes installed, one 5/8" (x/L = .031) downstream from cavity lip and the other 1 19/32" upstream from downstream edge (x/L = .92) Both sensors placed at y=0.

Simulated analog filter controller with the analog-sim program. Experiments run with different gain and delay settings at M = 0.34. Systematic sweeps in gain (0 – 5.5) with time delay held constant.
Systematic sweeps in time delay (.000 - .0032s) with gain fixed at 3 and 1.2, M = .34
Calibration (Transfer function) of actuator with B&K microphone and hot-film probe. White noise input and frequency sweeps input with function generator.

June 21, 2001 (Thursday)
Open-loop frequency sweeps with external signal added to feedback signal. Output signal from digital controller goes directly to channel 4 input, bypassing anti-aliasing filter.
2Vpp amplitude to open-loop signal. Optimized control with FGP (filtergainphase) digital controller. Frequency = 100Hz – 500Hz, M = 0.34.
Over controlled cases with frequency sweeps from 100 Hz –500 Hz, M = 0.34
No-control open loop forcing from 100 Hz – 500 Hz, M = 0.34.
Change to M = 0.45 for multi-mode suppression experiments.
Actuator calibration experiments white noise and frequency sweeps with flow on in the wind tunnel, M =.15, .2, slow flow.

June 22, 2001 (Friday)
Calibrate actuator system with frequency sweeps at different amplitudes.
Tests of different digital filter designs, with varying bandwidths, gains and delays.
Open loop forcing at 380Hz with voltage amplitudes ranging from 0.1 to 1 Vpp.
Open loop forcing with frequency sweeps from 40 Hz to 600 Hz in 20Hz increments, voltage at 1.0 Vpp.
Three tests of high frequency forcing at 1500 Hz, 1200 Hz, 1000 Hz.
Multi-band digital control experiment, M = .34, .375
Square wave input at 1Hz to create impulse-like disturbances.
Hot-film calibration coefficients

9. Figure List

Fig. 1. – Block diagram of adaptive feed-forward control algorithm.

Fig. 2 – Photograph of cavity in Subsonic Wind tunnel and hot film probes at upstream and downstream locations.

Fig. 3 - The cavity was instrumented with eight Kulite sensors (model XCS-093) positioned from the front wall to the rear wall along the centerline of the cavity.

Fig. 4 - The response functions of the actuator are reproduced in Fig. 4 from Ref.[16].

Fig. 5 – Rossiter mode diagram as function of Mach number.

Fig. 6 – Spectra at M = .25, .275, .35, .375 demonstrating single-mode and multi-mode behavior.

Fig. 7 – Rossiter modes superposed with normal cavity modes. Points of intersection coincide with single mode behavior.

Fig. 8 - Hot wire measurements of the shear layer velocity profiles. A) mean velocity; b) r.m.s. velocity for x/L = 0.1 to 0.6.

Fig. 9 - Growth of the shear layer is shown as momentum thickness vs. downstream distance with and without control.

Fig. 10a - The linear response of the shear layer velocity to the voltage input to the actuator.

Fig. 10b - The pressure response in the cavity relative to the velocity fluctuation level in the shear layer is shown in Fig.10b, and can be seen to have a nonlinear behavior.

Fig. 11 – Block diagram of the analog control system

Fig. 12 – Spectrum of pressure oscillations in the L/D = 5 cavity obtained at M=0.34. The dashed-line is the uncontrolled spectrum, and the solid line shows the result of closed-loop control with the unsteady bleed actuator.

Fig. 13 – Enhancement of second Rossiter mode 'B' suppresses energy in third Rossiter mode 'C'. The dashed line shows the uncontrolled baseline spectrum.

Fig. 14 – Suppression of second Rossiter mode 'B' enhances energy in third Rossiter mode 'C' and suppresses the fourth mode 'D'. The dashed line shows the uncontrolled baseline spectrum.

Fig. 15 – Suppression of third Rossiter mode enhances energy in second Rossiter mode and slightly suppresses the first mode. This establishes a connection between odd modes. The dashed line shows the uncontrolled baseline spectrum.

Fig. 16 – Multiple passbands in the feedback signal allow multiple modes to be suppressed simultaneously.

Fig. 17 – Cancellation path model used for single mode suppression with adaptive controller at M = 0.34

Fig. 18 – Spectrum at M = 0.34 with digital control

Fig. 19 – Coherence between feedback and reference signal M = 0.34

Fig. 20 – Spectrum of multimode control with digital adaptive control.

Fig. 21 – Block diagram of Rowley's flow physics model.

Fig. 22 – Experimentally measured transfer function for shear layer

Fig. 23 – Transfer function representative of scattering process.

Fig. 24 – Transfer function for acoustic modes.

Fig. 25 – Transfer function for receptivity model.